leading to ectopic bone formation. By contrast, the overexpression of HDAC4 in proliferative chondrocytes inhibited chondrocyte hypertrophy (Vega et al., 2004).

The transcription factor RUNX2 (CBFA1) is a key regulator of osteoblast differentiation. When RUNX2-deficient mice were generated, a lack of chondrocyte hypertrophy was found, suggesting that RUNX2 might regulate chondrocyte hypertrophy as does HDAC4 (Komori et al., 1997). To address this possibility, non-hypertrophic chondrocyte-specific *Runx2* transgenic mice were generated. These animals showed ectopic chondrocyte hypertrophy and enhanced endochondral ossification (Takeda et al., 2001). MEF2C is a crucial transcription factor in muscle and cardiovascular development. To clarify its role in chondrogenesis, cartilage-specific conditional *Mef2c* deletion mice and cartilage-specific dominant-negative and dominant-active MEF2C mice were generated, and these demonstrated a positive role for MEF2C in chondrocyte hypertrophy (Arnold et al., 2007). Genetically, the mild phenotype in the sternum of $Mef2c^{+/-}$ pups was rescued by deletion of one copy of the *Hdac4* gene, demonstrating that it depends on a balance between transcriptional activation by MEF2C and repression by HDAC4 (Arnold et al., 2007). In addition, HDAC4 interacts directly with RUNX2 to repress its transcriptional activity on the type X collagen promoter (Vega et al., 2004). Therefore, HDAC4 is thought to be a central negative regulator of chondrocyte hypertrophy.

With regard to the regulation of HDAC4 activity in chondrocyte hypertrophy, a recent study proposed that phosphatase PP2A, which is activated by the PTHrP-cAMP-PKA cascade in chondrocytes, dephosphorylates HDAC4 to turn on its activity and to potentiate its localization in nuclei, thereby inhibiting chondrocyte hypertrophy (Kozhemyakina et al., 2009). However, the regulatory mechanisms that suppress the transcriptional repression activity of HDAC4 in chondrocytes have not been reported so far.

Salt-inducible kinase 3 (SIK3, also known as QSK) is a member of the 5′-AMP-activated protein kinase (AMPK) family. SIK3 belongs to the SIK subfamily, which also includes SIK1 (also known as MSK or SNF1LK) and SIK2 (also known as QIK) (Katoh et al., 2004). Mammalian SIK1 and SIK2 are currently being characterized in terms of their function in various biological processes and molecular regulatory mechanisms. Recently, fly SIK3 (the homolog of mouse SIK2) was shown to sequester HDAC4 in the cytoplasm and to regulate the energy balance in the *Drosophila* fat body (Wang et al., 2011). Compared with SIK1 and SIK2, the function of SIK3 is poorly understood. To understand SIK3 function in vertebrates, we generated SIK3-deficient mice. The SIK3-deficient mice showed various phenotypes, including bone abnormalities (this study) and impaired cholesterol metabolism (T.U., Y. Itoh, O. Hatano, A. Kumagai, M. Sanosaka, T. Sasaki, S.S., J. Doi, K. Tatsumi, K. Mitamura et al., unpublished). Here, we report a role for SIK3 in skeletal development. By performing anatomical and histological analyses, we clarified that the bone abnormalities in SIK3-deficient mice are due to impaired chondrocyte hypertrophy. We also demonstrated that SIK3 binds directly to HDAC4 and has the capacity to anchor HDAC4 in the cytoplasm. Together, our results establish SIK3 as an essential factor for chondrocyte hypertrophy.

MATERIALS AND METHODS

Generation of *Sik3* knockout mice and embryos

The *Sik3* knockout strategy and targeting vector design are shown in supplementary material Fig. S1. Briefly, the PGK-neo cassette was inserted in place of exon 1 of *Sik3*. The successful targeting of embryonic stem cells was confirmed by Southern blot analysis, and the cells were injected into C57BL/6N blastocysts. To obtain SIK3-deficient embryos, *Sik3* heterozygous male and female mice were mated and wild-type littermates were used as controls.

Generation of *Col11a2-hSIK3* transgenic mice

The α2(XI) collagen gene-based expression vector 742LacZInt contains the mouse *Col11a2* promoter (–742 to +380), an SV40 RNA splice site, the *lacZ* reporter gene, SV40 polyadenylation signal and a 2.3 kb segment of the first intron of *Col11a2* as an enhancer (Tsumaki et al., 1996). To create the human *SIK3* (*hSIK3*) transgene, the *hSIK3* fragment was cloned into the expression vector, replacing the *lacZ* gene, to create *Col11a2-hSIK3*. Transgenic mice were produced by microinjection of the linearized insert into the pronuclei of fertilized eggs from F1 hybrid mice (C57BL/6 × DBA), as described previously (Hiramatsu et al., 2011). Transgenic mice were identified by PCR assays on genomic DNA extracted from the tail. The mice were backcrossed at least eight times to the C57BL/6N strain.

All experiments were approved by the Institutional Animal Care and Use Committee (IACUC) of Osaka University Graduate School of Medicine and the Osaka University Living Modified Organism (LMO) Experiments Safety Committee.

Cartilage and bone staining

For whole-mount skeletal analysis, mice or embryos were skinned, the internal organs and as much connective tissue as possible, including muscles and tendons, were removed, and the specimens fixed overnight in pure ethanol. The specimens were stained with Alcian Blue and Alizarin Red for 48 hours for embryos or 72 hours for adult mice. After staining, embryos were incubated in 20% glycerol in a 1% KOH solution and adult specimens were incubated in 3% KOH solution at 37°C for 1 day to remove soft tissue. To improve transparency, specimens were cleared in 50% glycerol in a 0.5% KOH solution at 37°C for 2 days, which was then replaced with 80% glycerol solution for completion of the reaction.

Sectioning and staining

For juvenile and adult mouse samples, specimens were fixed in 10% phosphate-buffered formalin at 4°C for 16-24 hours, followed by decalcification with saturated EDTA solution for 4 days. For embryonic samples, specimens were fixed in 4% PFA in PBS at 4°C for 16 hours, followed by decalcification with saturated EDTA solution for 1 day, except for specimens younger than E18.5 and samples used for von Kossa staining. The samples were embedded in paraffin, sectioned at 3 μm, and then subjected to Safranin O and Fast Green staining or von Kossa staining according to standard protocols.

Immunofluorescent and immunohistochemical staining

Antibodies used for the immunofluorescent analysis of section samples were as follows: mouse anti-type I collagen (Abcam, 1:500), mouse anti-type II collagen (Thermo Scientific, 1:500), mouse anti-type X collagen (Quartett, 1:100), goat anti-MMP13 (Millipore, 1:100), rabbit anti-SOX9 (Santa Cruz Biotechnology, 1:100), mouse anti-PCNA (Santa Cruz, 1:100), rabbit anti-SIK3 (Abcam, 1:100), rabbit anti-HDAC4 (Abcam, 1:100), rabbit anti-MEF2C (Abcam, 1:100), Alexa Fluor-conjugated secondary antibodies (Invitrogen, 1:500) and an HRP-labeled secondary antibody (GE Healthcare, 1:500).

Deparaffinized specimens were incubated in 20 mM Tris-HCl (pH 9.0) at 70°C for 6 hours to retrieve the antigen. For detection of type II collagen, samples were treated with 20 μM proteinase K for 10 minutes at 37°C. After blocking with 2% blocking reagent (Roche), the specimens were stained with primary antibody at 4°C overnight, then rinsed twice with PBS, and stained with a secondary antibody for 2 hours, followed by nuclear counterstaining with Hoechst 33342 (Invitrogen, 1:1000) for 30 minutes or, for samples used for detection of type II collagen, with Hematoxylin at room temperature. Specimens were observed using a fluorescence microscope system (Eclipse Ti, Nikon) equipped with a CCD camera (Hamamatsu Photonics). HRP labeling was visualized with DAB reagent (DAKO).

Cell culture, transfection, pulldown assay and imaging

293FT cells were grown in DMEM containing 10% FBS. ATDC5 cells were grown in DMEM/F-12 medium containing 5% FBS. The *Hdac4* and *Mef2c* cDNAs were cloned from a primary chondrocyte cDNA pool into the pENTR vector (Invitrogen) and their sequences confirmed. The primer sequences used for cloning are listed in supplementary material Table S1. Full-length *Sik3* cDNA was purchased from Invitrogen. For HA-tagged HDAC4 expression, *Hdac4* cDNA was subcloned into the pCMV-HA expression vector (Clontech). To construct an EGFP- HDAC4 fusion expression vector, the *Egfp* gene was subcloned into the 5′ region of the *Hdac4* gene in pENTR-Hdac4. For other expression constructs, the cDNAs were transferred into the CMV-driven expression vector using the Gateway system (Invitrogen). For transient transfection, Lipofectamine 2000 (Invitrogen) was used according to the manufacturer's instructions.

The pulldown assay was performed as described previously (Takeda et al., 2006). Briefly, transiently transfected cells were solubilized in RIPA buffer containing protease inhibitor and phosphatase inhibitor (both Roche) 48 hours after transfection. The cell lysates in RIPA buffer were subjected to pulldown assay with the 12CA5 anti-HA or 9E10 anti-Myc antibody (Santa Cruz) and Protein G Sepharose beads (GE Healthcare), were separated on a NuPAGE gel (Invitrogen) and evaluated by a western blotting analysis with the ECL system (PerkinElmer). A ChemiDoc XRS Plus system (BioRad) was used for image development.

For cellular immunofluorescence imaging, cells were fixed in 10% PFA for 30 minutes at room temperature, washed twice with PBS, and then permeabilized with 0.2BT solution (0.2% Triton X-100 and 2 mg/ml BSA in water) for 10 minutes. The specimens were stained with anti-SIK3 antibody (1:500) for 2 hours, followed by an Alexa Fluor-conjugated secondary antibody (1:2000) for 1 hour, and were then counterstained with Hoechst 33342 (1:1000) for 30 minutes at room temperature. The cells were imaged using a fluorescence microscope (Eclipse Ti) equipped with a CCD camera (Hamamatsu Photonics).

MEF2C luciferase reporter assays were performed as described previously (Takemori et al., 2009). The constitutively active form of SIK3 (T163E, S494A) (Katoh et al., 2006) was used in the ATDC5 cells.

Quantitative PCR

Humeri were isolated from E18.5 embryos and tissues were crushed by vigorous shaking with beads. Total RNA was purified using an RNA purification kit (Qiagen). For cDNA synthesis, Superscript III (Invitrogen) was used according to the manufacturer's protocol. The primers used are listed in supplementary material Table S1. The PCR reaction was performed with CYBR premix reagent (TaKaRa) and the 7900HT Fast Real-Time PCR system (Applied Biosystems).

Statistical analysis

Statistically significant differences between groups were evaluated by Student's *t*-test. $P<0.05$ was considered statistically significant. The analyses were performed using Excel (Microsoft) and Statcel3 (OMS Publishing).

RESULTS

SIK3-deficient mice have skeletal defects

Although $Sik3^{-/-}$ mice were born at the expected Mendelian frequency, 90% died on the first day after birth (T.U., Y. Itoh, O. Hatano, A. Kumagai, M. Sanosaka, T. Sasaki, S.S., J. Doi, K. Tatsumi, K. Mitamura et al., unpublished). The surviving SIK3-deficient mice showed dwarfism throughout their postnatal life. The mean weight of $Sik3^{-/-}$ mice was 7 g, whereas that of $Sik3^{+/+}$ and $Sik3^{+/-}$ mice was 13 g at 3 weeks of age. Because an X-ray analysis revealed that they had bone deformities, we focused on the skeletal abnormality as a SIK3-deficient phenotype. Anatomical examination of SIK3-deficient mice revealed numerous skeletal abnormalities (Fig. 1). When each of the skeletal elements of SIK3-deficient mice (4 months old) were compared with those of age-matched wild-type mice, we found that they had a shorter sternum

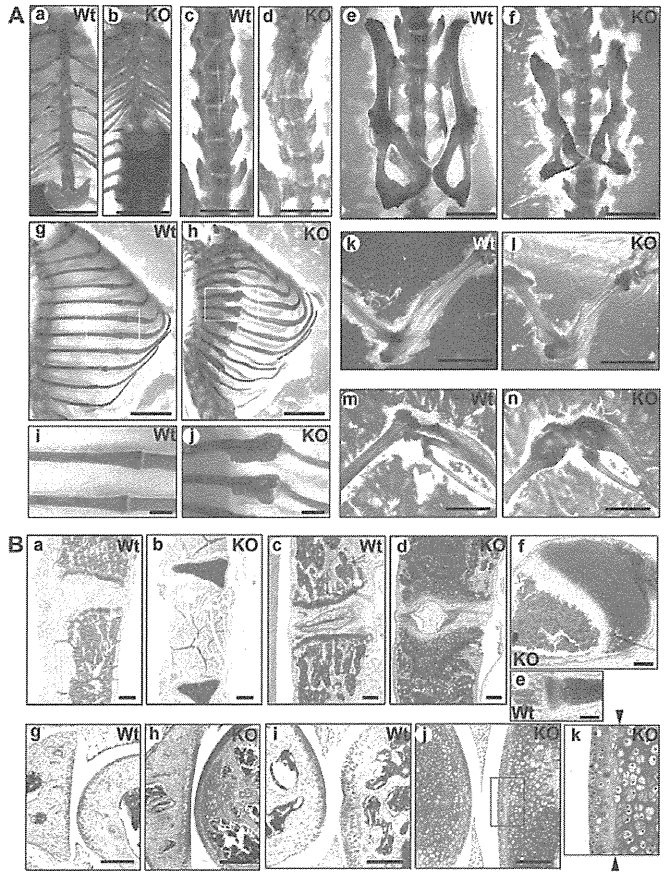

Fig. 1. Skeletal deformity in SIK3-deficient mice. (**A**) Skeletal elements from wild-type (Wt) and SIK3-deficient (KO) mice at 4 months of age stained with Alizarin Red and Alcian Blue: sternum (a,b), spine (c,d, front view), pelvis (e,f), ribcage (g,h, lateral view) and each junction (i,j), elbow (k,l) and knee (m,n). (**B**) Histological sections from wild-type and SIK3-deficient mice at 4 months of age (except for the rib junction, which was examined at 3 months of age) stained with Safranin O, Fast Green and Iron Hematoxylin: sternum (a,b), spine (c,d), rib junction (e,f), elbow (g,h) and knee (i,j), and a higher magnification view of articular cartilage regions of the knee (k). Arrowheads indicate the tide line. Scale bars: 5 mm in Aa-h; 1 mm in Ai,j; 200 μm in B.

with low mineralization (Fig. 1Aa,b), a thinner spine that was twisted as in scoliosis (Fig. 1Ac,d), a hypoplastic pelvis (Fig. 1Ae,f), short mineralized ribs with an abnormal mass at the junction between the bone and cartilage, which was similar in appearance to a rachitic rosary (Fig. 1Ag-j), and shorter long bones (Fig. 1Ak,l) with epiphyseal and metaphysial expansion of the limb joint region (Fig. 1Am,n). In SIK3-deficient mice, delayed membranous ossification of the skull bones was observed on postnatal day (P) 1 (supplementary material Fig. S2A,B). The parietal bone had an immature appearance from the juvenile stage until 8 months of age (supplementary material Fig. S2C-H, asterisks) and the sutures remained loosely closed throughout adulthood (supplementary material Fig. S2C-H, arrowheads). A large fontanelle remained open from juvenile stage until adulthood (supplementary material Fig. S2C-H, arrows), whereas it was already closed in 3-week-old wild-type mice. The skeletal abnormalities, especially the rachitic rosary-like structures in the ribs and unclosed large fontanelle, were reminiscent of rickets.

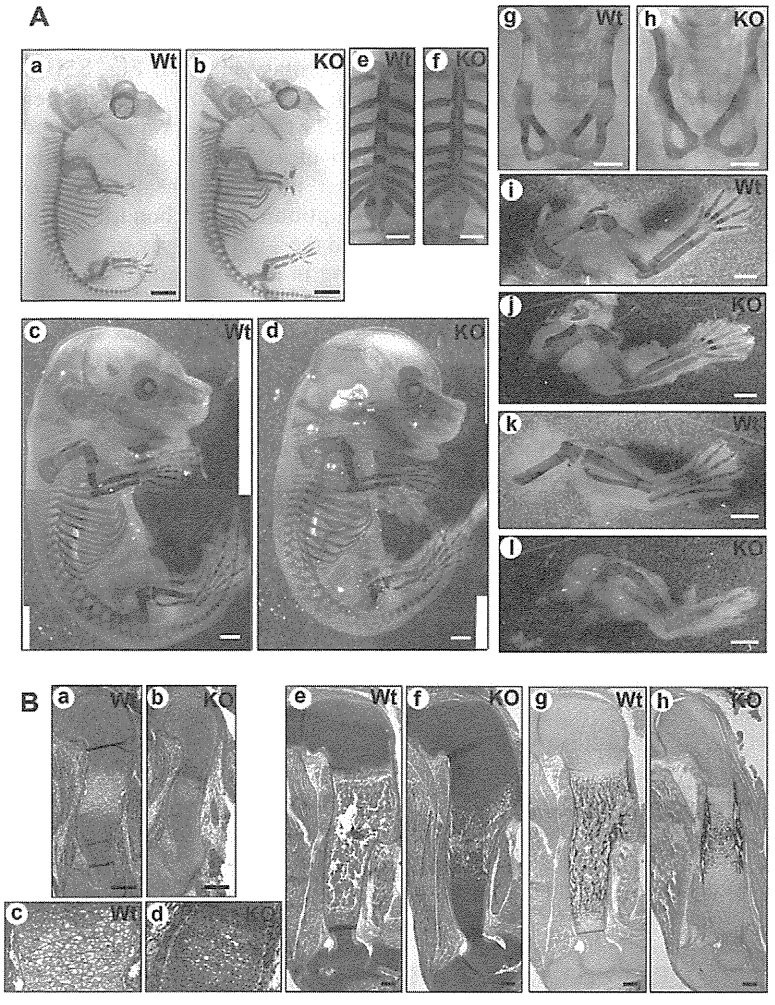

Fig. 2. Impaired chondrocyte hypertrophy in SIK3-deficient mouse embryos. (**A**) Wild-type and SIK3-deficient (KO) skeletons stained with Alizarin Red and Alcian Blue at E14.5 (a,b), E15.5 (c,d) and E18.5 (e-l): whole skeleton (a-d), sternum (e,f), pelvis (g,h), forelimb skeleton (i,j) and hindlimb skeleton (k,l). (**B**) Histological sections from wild-type and SIK3-deficient embryos stained with Safranin O, Fast Green and Iron Hematoxylin (a-f) or with von Kossa and Eosin (g,h) at E14.5 (a-d) and E18.5 (e-h). Scale bars: 1 mm in A; 200 μm in B.

In addition, SIK3 expression was detected in the kidney and liver, in which the effects of SIK3 deletion were also marked (T.U., Y. Itoh, O. Hatano, A. Kumagai, M. Sanosaka, T. Sasaki, S.S., J. Doi, K. Tatsumi, K. Mitamura et al., unpublished). Renal disorders produced by physical damage or chemical treatment sometimes induce osteomalacia, accompanied by low calcium and/or low phosphorus levels in the serum. Therefore, we measured the concentrations of calcium and phosphorus in the serum, and found that both were almost normal in SIK3-deficient mice (supplementary material Fig. S3). Thus, we excluded the possibility that the skeletal abnormalities of SIK3-deficient mice were due to impaired metabolism of phosphorus or calcium.

Accumulation of cartilage in SIK3-deficient mice

To further investigate the bone malformation in SIK3-deficient mice, we histologically analyzed the interior of the bones of 3-month-old (rib) or 4-month-old (other bones) mice. Safranin O staining revealed marked cartilage accumulation in most of the bones of SIK3-deficient mice. In the sternum, the cartilage region did not separate, and there was absolutely no bone marrow space (Fig. 1Ba,b). In the spine, expanded cartilage tissue and a malformed intervertebral disk were found (Fig. 1Bc,d). SIK3-deficient ribs were half filled with cartilage (Fig. 1Be,f). The epiphysis and metaphysis of the limb bones of SIK3-deficient mice were filled with cartilage bulk and displayed small secondary ossification centers (Fig. 1Bg-j, supplementary material Fig. S4C,D), whereas a well-differentiated secondary ossification center was developed in wild-type mice by 3 weeks of age. Although separation between the articular cartilage and the growth plate cartilage was found in 4-month-old SIK3-deficient mice, the secondary ossification center was not well developed even by 8 months of age (supplementary material Fig. S4C-L). In the articular cartilage of SIK3-deficient mice, the zone below the tidemark was thickened. The Safranin O staining intensity and cell morphology in the zone above the tidemark of articular cartilage were similar in SIK3-deficient and wild-type mice (Fig. 1Bk). Collectively, these findings indicate that impaired chondrocyte metabolism was fundamental to the skeletal abnormalities of SIK3-deficient mice.

Impaired chondrocyte hypertrophy in SIK3-deficient embryos

To pinpoint the onset of the skeletal abnormalities in SIK3-deficient mice we next surveyed skeletal development at various embryonic stages by Alcian Blue/Alizarin Red staining. Neither skeletal malformation nor homeotic transformation was observed in SIK3-deficient embryos at E14.5, indicating that *Sik3* gene deletion did not affect the chondrogenic commitment of mesenchymal cells or skeletal patterning (Fig. 2Aa,b). In wild-type mouse embryos, bone mineralization was indicated by Alizarin Red staining in several skeletal elements by E15.5. Compared with wild-type embryos, delayed mineralization of the ribs, the long bones in the limbs and cervical bones was observed in SIK3-

deficient embryos at E15.5 (Fig. 2Ac,d). By E18.5, the mineralization at most skeletal elements that are developed through endochondral bone formation had progressed in wild-type embryos. By contrast, SIK3-deficient embryos displayed delayed bone mineralization. The sternum and vertebrae remained uncalcified (Fig. 2Ae-h). The mineralized regions at the pelvis (Fig. 2Ag,h), the scapula and the long bones of the forelimb and hindlimb (Fig. 2Ai-l) were markedly reduced in SIK3-deficient embryos as compared with wild-type embryos at E18.5. By contrast, the shape and size of the cartilage in the epiphyseal and metaphysial regions of the limbs were almost normal in SIK3-deficient embryos (Fig. 2B). In spite of the reduced mineralization, the length of the long bones in the limbs was almost the same in SIK3-deficient and wild-type embryos (supplementary material Fig. S5A). Reflecting this finding, the body size of newborns was indistinguishable between genotypes (supplementary material Fig. S1C). After birth, bone elongation in the SIK3-deficient mice was restricted, and the length of the long bones in the limbs was obviously shortened at 6 weeks of age (supplementary material Fig. S5A).

A further histological analysis revealed a definitive primary defect of the cartilage in SIK3-deficient embryos. A cluster of well-differentiated hypertrophic chondrocytes is initially observed at the center of the humerus in wild-type embryos at E14.5. By contrast, only a few partially differentiated chondrocytes were observed at the center of the humerus in SIK3-deficient embryos at E14.5 (Fig. 2Ba-d). Therefore, we speculated that a disturbance of chondrocyte hypertrophy was the point at which SIK3 deficiency affected skeletal development. At E18.5, the first ossification center is well formed in the central region and the cartilage region is restricted at both ends in the wild-type mouse humerus. By contrast, the humerus of SIK3-deficient embryos was almost completely filled with cartilage tissue and the small first ossification center was barely recognizable (Fig. 2Be,f).

To characterize the cartilage tissue that accumulated in the humerus of SIK3-deficient embryos, we examined the expression of several structural markers of cartilage (types I, II and X collagen) at E18.5. We confirmed that the accumulated cartilage tissue was type I collagen-negative and type II collagen-positive, indicating that the tissue was bona fide cartilage tissue, consistent with the intense Safranin O staining (supplementary material Fig. S6A). Type X collagen, a hypertrophic structural marker, was only weakly detected at the center of the SIK3-deficient humeri, reflecting a disturbance in chondrocyte hypertrophy (supplementary material Fig. S6A). A further analysis based on cell morphology revealed that the round chondrocyte zone was of normal length but that there was an extended flat columnar chondrocyte zone and post-flat chondrocyte zone in SIK3-deficient compared with wild-type humeri at E18.5 (supplementary material Fig. S7). By assessing the expression of PCNA, it was confirmed that most of the accumulated flat chondrocytes were in a proliferative state (supplementary material Fig. S8).

In spite of the disruption of chondrocyte hypertrophy, significant mineralization, as confirmed by von Kossa staining, was observed at the bone collar of the humerus in SIK3-deficient embryos at E18.5, and it was apparently thicker than that in wild-type embryos (Fig. 2Bg,h). A real-time RT-PCR analysis showed that the genes encoding the mineralization factors ANK and ENPP were expressed at E18.5 in SIK3-deficient humerus, although the expression levels were slightly reduced (supplementary material Fig. S5B). The expression levels of the genes encoding the vascularization factors VEGF and VEGFR and the hypoxia inducible factors HIF1α and HIF2α (EPAS1 – Mouse Genome Informatics) were similar in wild-type and SIK3-deficient humeri (supplementary material Fig. S5B). A similar phenomenon has been reported in *Sox9* transgenic embryos, in which chondrocyte hypertrophy was suppressed (Akiyama et al., 2004; Hattori et al., 2010). These findings suggest that there is a system that compensates for bone mineralization in cases of disruption of endochondral skeletal development. We also performed the TUNEL assay to determine whether apoptosis was occurring in the accumulating cartilage tissue in SIK3-deficient embryos and juvenile mice. Few TUNEL-positive cells were detected in the accumulating cartilage tissue of E18.5 and juvenile specimens (supplementary material Fig. S8), suggesting that the accumulated chondrocytes in SIK3-deficient mice were not actively removed but remain alive until entry into hypertrophy upon differentiation.

Although the SIK3-deficient humerus was filled with chondrocytes at E18.5 (Fig. 2Be,f), first and secondary ossification centers were eventually formed (supplementary material Fig. S4) and mineralization occurred (Fig. 1A) with increasing age. These results suggested that the chondrocyte hypertrophy program was diminished rather than completely abolished. In order to clarify whether the post-hypertrophic program was still functional, we analyzed the expression of MMP13, a post-hypertrophic marker (Mitchell et al., 1996), and of SP7 (osterix), an osteogenesis marker (Nakashima et al., 2002), in juvenile epiphyseal tibia specimens. Consistently, expression of these markers was observed, although their expression patterns were somewhat disorganized compared with the wild-type tissues (supplementary material Fig. S6B). Taken together, it was concluded that the major effect of SIK3 deficiency on skeletal development was disruption of chondrocyte hypertrophy.

Expression of SIK3 in hypertrophic chondrocytes

Based on a histological analysis, we revealed that SIK3 deficiency results in the disruption of chondrocyte hypertrophy (Figs 1, 2). To address the endogenous SIK3 expression pattern in cartilage tissue, we performed immunofluorescent staining for SIK3 in wild type. Consistent with the histological results, endogenous SIK3 was detected in both prehypertrophic and hypertrophic chondrocytes, and it was localized in the cytoplasm of cells in the humerus at E18.5 (Fig. 3Aa,b), scapula at E15.5 (Fig. 3Ac,d) and growth plate of the knee at 3 weeks of age (Fig. 3Ae,f).

Previously, it was revealed that HDAC4 and MEF2C are central regulators of chondrocyte hypertrophy and skeletogenesis and that HDAC4 functions as a transcriptional repressor for MEF2C and RUNX2 (Vega et al., 2004; Arnold et al., 2007). Other studies have also reported interactions between SIK1/2 and HDACs (van der Linden et al., 2007; Takemori et al., 2009). We therefore hypothesized that SIK3 might exert its effect via HDAC4 to regulate the activities of MEF2C and RUNX2 in chondrocyte hypertrophy. To evaluate this hypothesis, we first immunohistochemically analyzed the expression of SOX9, HDAC4 and MEF2C (as a representative target of HDAC4) in the wild-type humerus at E15.5 (Fig. 3B). As previously reported, SOX9 was detected in the proliferative and in some of the prehypertrophic chondrocytes and was undetectable in hypertrophic chondrocytes (Fig. 3Bc,d). Expression of MEF2C and HDAC4 was detected in both the prehypertrophic and hypertrophic chondrocyte regions (Fig. 3Be-h). The expression of SIK3 was exclusive to cells that also expressed SOX9 and was similar to that of HDAC4 (Fig. 3Bi,j).

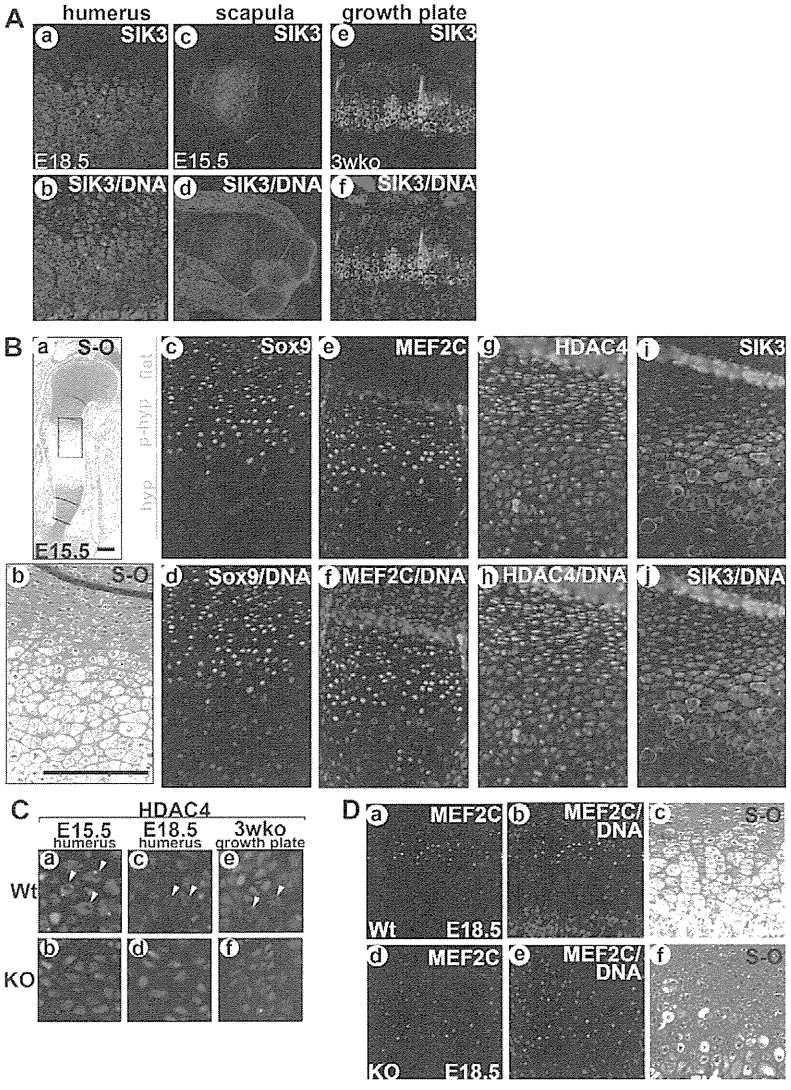

Fig. 3. Expression patterns of SIK3 and chondrocyte hypertrophic factors. (**A**) Immunofluorescent staining for SIK3 (red) in the humerus (a,b), scapula (c,d) and growth plate of the proximal tibia of 3-week-old (e,f) wild-type mice. Nuclei were counterstained with Hoechst 33342 (blue). SIK3 expression was detected in prehypertrophic and hypertrophic chondrocytes and was localized in the cytoplasm in all tissues analyzed. (**B**) A comparison of the expression patterns of SIK3 and chondrocyte hypertrophic factors in the humerus of wild-type embryos (E15.5). Bright-field views of a section stained with Safranin O, Fast Green and Hematoxylin are shown (a,b). Serial sections were stained with anti-SOX9 (c,d), anti-MEF2C (e,f), anti-HDAC4 (g,h) or anti-SIK3 (i,j) antibodies and an Alexa Fluor-conjugated secondary antibody. Scale bars: 200 μm. (**C**) Immunofluorescent staining for HDAC4 in the humerus at E15.5 (a,b) and E18.5 (c,d) and in the growth plate of the proximal tibia at 3 weeks of age (e,f) of wild-type (a,c,e) and SIK3-deficient (b,d,f) mice. Arrowheads indicate cells in which HDAC4 was excluded from the nucleus. However, HDAC4 persisted in the nucleus in the SIK3-deficient specimens. (**D**) Immunofluorescent staining for MEF2C in the humerus at E18.5 in wild-type (a,b) and SIK3-deficient (d,e) embryos. Semi-serial sections were stained with Safranin O, Fast Green and Hematoxylin (c,f).

We also found that there was a shift in the subcellular localization of HDAC4 to the cytoplasm in hypertrophic chondrocytes, where the expression of MEF2C was strong in the nuclei. The translocation of HDAC4 was observed at the hypertrophic chondrocyte zone in the humerus of E15.5 and E18.5 embryos and in the growth plate of 3-week-old wild-type mice (Fig. 3C). By contrast, HDAC4 translocation to the cytoplasm was seldom observed in chondrocytes at the corresponding region in SIK3-deficient embryos and mice. However, although the location was not synchronized, significant MEF2C-positive cells were observed at the edge of the accumulated cartilage in SIK3-deficient humeri, despite the fact that chondrocyte hypertrophy had not progressed (Fig. 3Dd-f). We therefore concluded that the HDAC4 remaining in the nuclei of the SIK3-deficient chondrocytes continued to repress MEF2C activity, resulting in the blockage of chondrocyte hypertrophy. Taken together, these data indicated that SIK3 is required for HDAC4 translocation to the cytoplasm during chondrocyte hypertrophy.

SIK3 forms a complex with HDAC4 to regulate its subcellular localization

To address how SIK3 regulates the subcellular localization of HDAC4, we performed a co-immunoprecipitation assay to determine whether they form a complex. The co-immunoprecipitation assay with knee lysates from 2-week-old mice indicated that a complex was indeed formed between HDAC4 and SIK3 (Fig. 4A). To further analyze the regulation of HDAC4 by SIK3 in vitro, HA-tagged HDAC4 and SIK3 expression vectors were co-transfected into 293FT cells, lysed, and assayed with an anti-HA antibody. This confirmed that HDAC4 and SIK3 form a complex (Fig. 4B). Using this system, we explored the binding domains of SIK3 and HDAC4 required for complex formation, and identified the kinase domain (amino acids 1-270) of SIK3 and the central region (amino acids 351-620) of HDAC4 as binding domains (supplementary material Fig. S9).

We next examined whether this interaction affects the subcellular localization of HDAC4. To monitor HDAC4 localization, an EGFP-tagged HDAC4 expression vector was transfected into 293FT cells with or without the SIK3 expression vector, and GFP was observed by fluorescence microscopy. In agreement with the expression pattern of endogenous SIK3 in hypertrophic chondrocytes (Fig. 3B), the overexpressed SIK3 was detected in the cytoplasm (Fig. 4C). When GFP-HDAC4 was overexpressed alone, GFP fluorescence was observed in the nucleus (Fig. 4D, upper panel). By contrast, when SIK3 was co-expressed, GFP fluorescence was observed in the cytoplasm (Fig. 4D, bottom panels). These results indicated that SIK3 can alter the localization

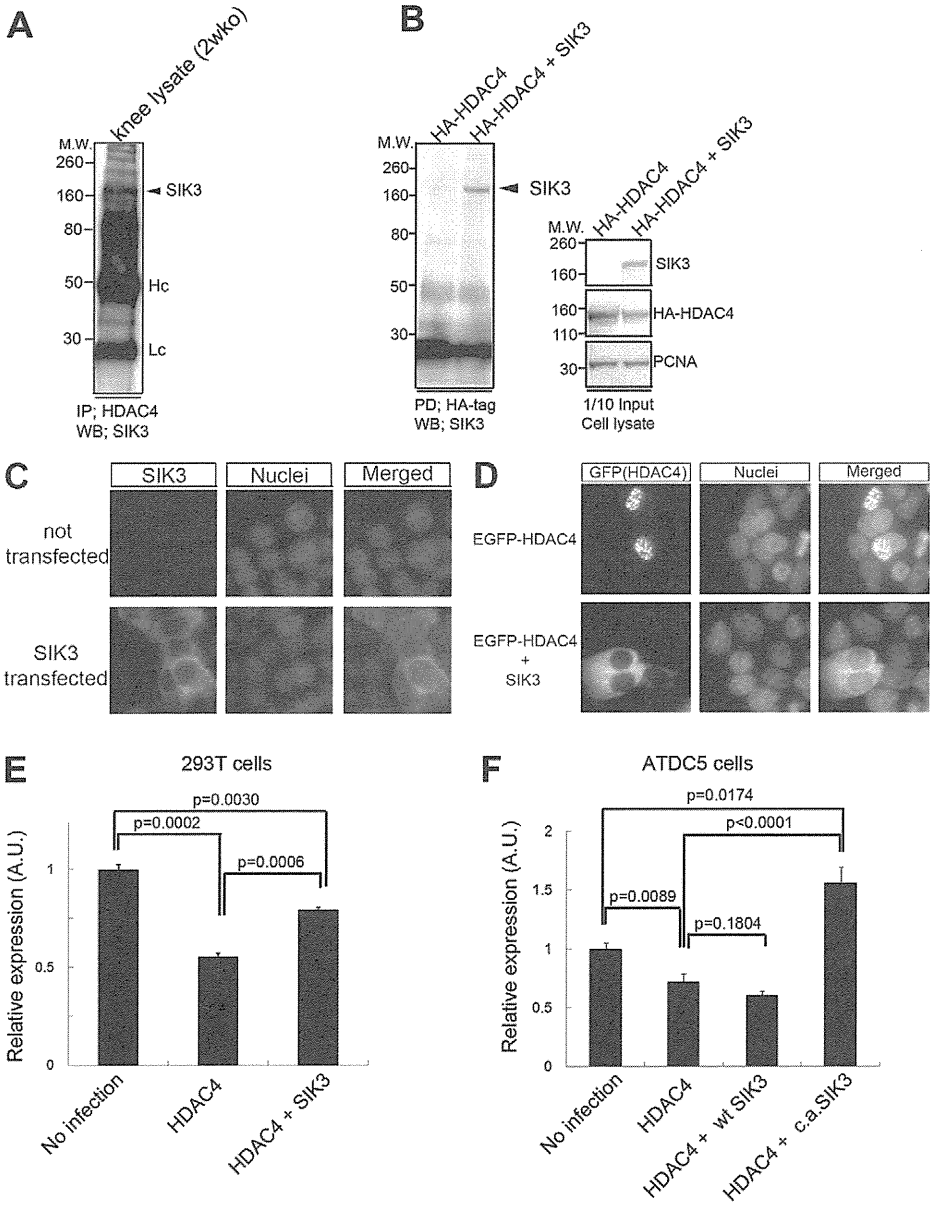

Fig. 4. Interaction of SIK3 with HDAC4 regulates its subcellular localization. (**A**) Co-immunoprecipitation of SIK3 with HDAC4. Knee tissue from 2-week-old mice was lysed and endogenous HDAC4 immunoprecipitated. Co-immunoprecipitated SIK3 was detected. Hc, IgG heavy chain; Lc, IgG light chain. (**B**) Pulldown assay of SIK3 with HA-HDAC4. 293FT cells were transiently transfected with expression vectors carrying SIK3 and HA-tagged HDAC4. Pulled-down samples (PD) and whole cell lysates (input) were subjected to SDS-PAGE followed by immunoblotting with the indicated antibodies. Left and right panels show the pulldown assay and the transiently expressed proteins, respectively. PCNA was monitored as a loading control. (**C**) SIK3 immunofluorescence. 293FT cells were transiently transfected with a SIK3 expression vector and stained 24 hours after transfection using an anti-SIK3 antibody followed by an Alexa Fluor-conjugated secondary antibody. A SIK3 signal was detected in the cytoplasm of transfected cells, whereas there was no substantial signal in non-transfected cells. (**D**) Translocation of HDAC4 by SIK3. A GFP-HDAC4 expression vector was transfected with or without a SIK3 expression vector into 293FT cells. When EGFP-HDAC4 was transfected alone, GFP fluorescence was detected in the nuclei (top panels). When EGFP-HDAC4 and SIK3 were co-transfected, GFP fluorescence was detected in the cytoplasm (bottom panels). Nuclei were counterstained with Hoechst 33342. (**E**) MEF2C transcriptional activity in 293FT cells. 293FT cells were transiently transfected with a MEF2C-luciferase reporter plasmid and an expression vector encoding MEF2C without (basal control) or with expression vectors for HDAC4 and/or wild-type SIK3. The luciferase activity was measured 48 hours after transfection. (**F**) MEF2C transcriptional activity in ATDC5 cells. ATDC5 cells were transiently transfected with a MEF2C-luciferase reporter plasmid and an expression vector encoding MEF2C without (basal control) or with expression vectors for HDAC4 and/or wild-type SIK3, or with a constitutively active form of SIK3 (T163E, S494A). Error bars indicate s.d.

of HDAC4 from the nucleus to the cytoplasm. We also performed a MEF2C luciferase reporter assay to monitor whether the HDAC4 translocation induced by SIK3 might relieve MEF2C activity from suppression by HDAC4. When MEF2C was co-expressed with HDAC4, the MEF2C reporter activity was suppressed. In addition, when SIK3 was co-overexpressed recovery of the luciferase activity was observed, although the recovery was not complete (Fig. 4E). In ATDC5 cells, a prechondrogenic cell line, constitutively active forms of SIK3 (T163E, S494A), but not wild-type SIK3, showed HDAC4 inhibitory activity, suggesting that

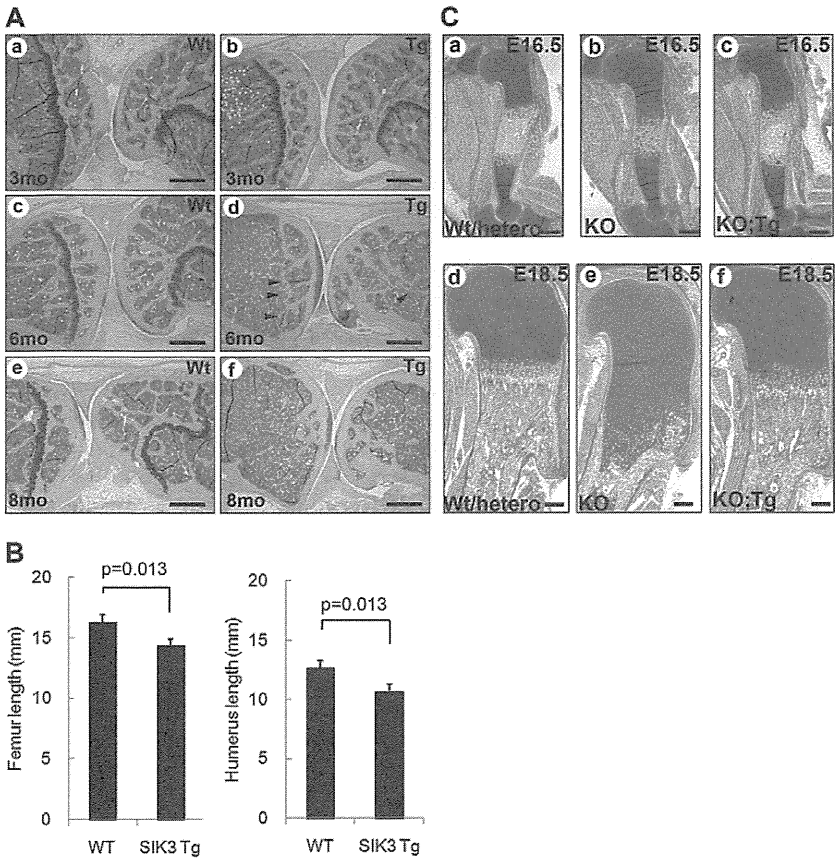

Fig. 5. Effects of forced expression of SIK3 in cartilage tissue. (**A**) Histological sections of the knee joint of wild-type and *Col11a2-hSIK3* transgenic mice stained with Safranin O and Fast Green. At 3 months of age, the growth plate of the transgenic mice appeared normal (a,b). By 6 months, the growth plate was starting to disappear (c,d) and by 8 months of age it had completely disappeared and the spongy bone was also starting to disappear (e,f). By contrast, the growth plates persisted in wild-type mice until they were 8 months of age. Arrowheads indicate the residual growth plates. (**B**) A comparison of the length of femur and humerus between wild-type and *hSIK3* transgenic (Tg) mice at 6 months of age. The *hSIK3* transgenic mice had shortened long bones. Error bars indicate s.d. (**C**) Transgenic rescue of SIK3. A $Sik3^{+/-}$ female mouse was mated with a $Sik3^{+/-}$; *Col11a2-hSIK3* transgenic male mouse and the embryos were dissected at E16.5 (a-c) or E18.5 (d-f). Chondrocyte accumulation in the SIK3-deficient proximal humerus was substantially restored by the *Col11a2-hSIK3* transgene. Scale bars: 500 μm in A; 200 μm in C.

ATDC5 cells lack factors that are required for the activation of SIK3 (Fig. 4F). Overall, these findings indicated that SIK3 anchors HDAC4 in the cytoplasm, thereby allowing MEF2C to be active.

Forced SIK3 expression in cartilage causes closure of the growth plate in adulthood

The expression of SIK3 in hypertrophic chondrocytes and impaired chondrocyte hypertrophy in SIK3-deficient embryos and mice indicate that SIK3 is indispensable for chondrocyte hypertrophy. We generated transgenic mice overexpressing human *SIK3* (*hSIK3*) specifically in chondrocytes under the control of *Col11a2* promoter/enhancer sequences (Tsumaki et al., 1996; Murai et al., 2008; Hiramatsu et al., 2011) to confirm the role of SIK3 in cartilage by a gain-of-function approach and to clarify that the phenotype of bone malformation in SIK3-deficient mice was really due to the cartilage tissue.

We previously demonstrated that GFP fluorescence driven by this system is detected only in the cartilage tissue during embryogenesis (Hiramatsu et al., 2011) and in both the articular and growth plate cartilage in adulthood (data not shown). To confirm the expression of the *hSIK3* transgene using this system, costal cartilage was harvested from postnatal pups at the P2 stage and subjected to SDS-PAGE, followed by immunoblotting with a SIK3 antibody (supplementary material Fig. S10). Although a dramatic effect of SIK3 overexpression was not observed during embryogenesis or during the juvenile period in *Col11a2-hSIK3* transgenic mice, we did observe the disappearance of the growth plate in the hind limbs with aging (Fig. 5A).

Generally, the growth plate is thought to comprise continually metabolizing chondrocytes, which are balanced in proliferation and differentiation (i.e. hypertrophy). Based on our findings, we speculated that the disappearance of the growth plate in cartilage-specific *hSIK3* transgenic mice occurred because the overexpressed SIK3 slightly accelerated the differentiation of chondrocytes at the growth plate, leading to chronic and excessive usage of chondrocytes and resulting in loss of the growth plate structure in older mice. Consistent with this hypothesis, the length of the long bones was reduced at 6 months of age (Fig. 5B) and the spongy bone structure was also beginning to disappear by 8 months of age in the *Col11a2-hSIK3* transgenic mice (Fig. 5A). Thus, we concluded that the disappearance of the growth plate in cartilage-specific *hSIK3* transgenic mice was a predictable phenotype for the gain-of-function approach for SIK3. In addition, the *Col11a2-hSIK3* transgenic/SIK3-deficient offspring displayed efficient rescue of the impaired chondrocyte hypertrophy phenotype at E16.5 (Fig. 5C, top panels) and at E18.5 (Fig. 5C, bottom panels). Nevertheless, despite the restoration of the bone phenotype, the lethality of SIK3 deficiency for newborn mice was not recovered, suggesting that bone deformity is not the primary cause of their postnatal death. Taken together, these results confirmed that the role of SIK3 in chondrocytes is to induce the progression of chondrocyte hypertrophy and that the impaired skeletal development of SIK3-deficient mice is due to the cartilage tissue.

DISCUSSION

Our study revealed that SIK3 is a crucial regulator of chondrocyte hypertrophy and identified the transcriptional regulator, HDAC4, as a target of SIK3 in chondrogenesis. SIK3-deficient mice displayed multiple phenotypes, including bone malformation with dwarfism, and these were concluded to be due to impaired chondrocyte hypertrophy. The abnormalities of the bone that develops via endochondral bone formation in

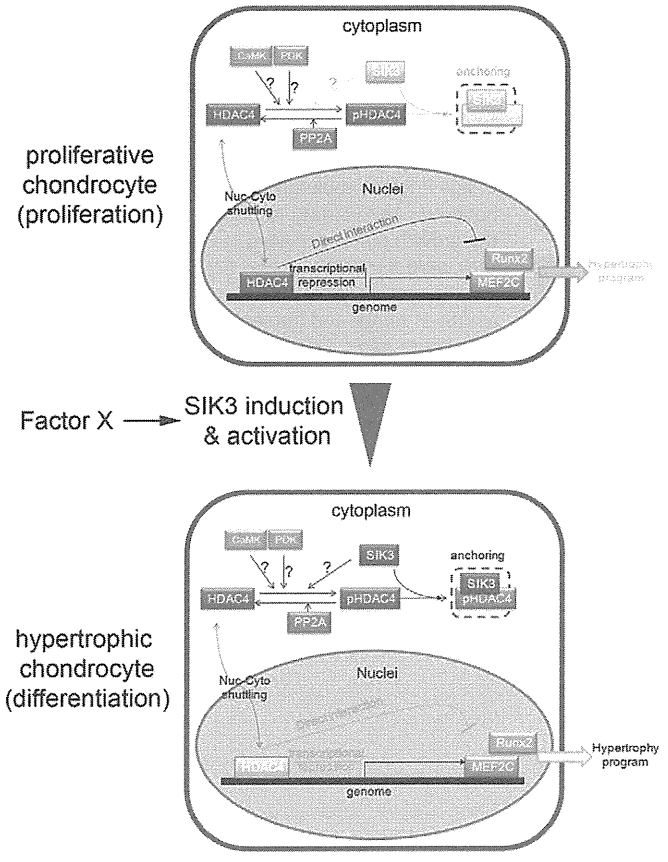

Fig. 6. Model depicting the role of SIK3 in chondrocyte hypertrophy. (Top) When SIK3 is absent, HDAC4 remains in the nucleus and epigenetically and mechanically represses MEF2C. (Bottom) Once SIK3 is induced, SIK3 binds to HDAC4 and anchors it in the cytoplasm, thereby allowing MEF2C to become active in the nucleus and facilitating the progression of the chondrocyte hypertrophic program. Question marks indicate possible phosphorylation activities opposing to PP2A, but not tested.

SIK3-deficient embryos were similar to those of cartilage-specific *Hdac4* transgenic embryos (Vega et al., 2004). Furthermore, our results showed that SIK3 forms a complex with HDAC4 and anchors it in the cytoplasm, thereby relieving MEF2C from transcriptional repression by HDAC4 in the nuclei. In conclusion, the regulation of HDAC4 by SIK3 is a crucial mechanism for the progression of chondrocyte hypertrophy during skeletal development (Fig. 6).

Expression of SIK3 in chondrocytes

SIK3-deficient mice were generated to better understand the physiological role of SIK3. We identified bone deformity with dwarfism as one of the phenotypes of SIK3-deficient mice. We found strong expression of SIK3 from prehypertrophic to hypertrophic chondrocytes during chondrogenesis and in the postnatal growth plate, suggesting the importance of SIK3 in chondrocyte hypertrophy. Indeed, SIK3-deficient embryos displayed impaired chondrocyte hypertrophy, which resulted in bone abnormalities. Furthermore, cartilage-specific *hSIK3* transgenic mice showed unnatural closure of the growth plate. As a result of our gain-of-function approach, it was demonstrated that the expression of additional SIK3 hastened chondrocyte hypertrophy and led to the depletion of non-hypertrophic chondrocytes, which are normally necessary to maintain the growth plate structure. Although the SIK3 expression pattern was consistent with its function in chondrocytes, further questions also arose. For example, it is unclear how and which transcription factor(s) regulate SIK3 expression in chondrocytes. So far, there have been few studies, but we intend to address this question in future studies to obtain a deeper understanding of the mechanism responsible for endochondral bone development.

Molecular mechanisms by which SIK3 exerts its activity in chondrocytes

One of the major findings of this study is that SIK3 regulates the subcellular localization of HDAC4, a negative transcriptional regulator of MEF2C and RUNX2 activity during chondrocyte differentiation, i.e. hypertrophy. For the first time, we revealed that SIK3 was strongly expressed from prehypertrophic to hypertrophic chondrocytes, in which HDAC4 was also expressed. In addition, we found that HDAC4 localization was shifted to the cytoplasm in wild-type chondrocytes, but that this seldom occurred in SIK3-deficient chondrocytes. In response to HDAC4 translocation, wild-type chondrocytes began hypertrophy. By contrast, chondrocyte hypertrophy was severely inhibited in spite of sufficient MEF2C expression in SIK3-deficient cartilage tissue. However, flat chondrocytes continued proliferating, maintaining their columnar structure and causing chondrocyte accumulation during development. These results suggested that SIK3 is required for proper chondrocyte hypertrophy and that its role is to change the subcellular localization of HDAC4 from the nucleus to the cytoplasm during chondrocyte differentiation.

Several studies have reported that SIK1 and SIK2 directly regulate HDACs (van der Linden et al., 2007; Takemori et al., 2009). Fly SIK3 (the homolog of mouse SIK2) has recently been shown to sequester HDAC4 in the cytoplasm and to regulate the energy balance in the *Drosophila* fat body (Wang et al., 2011). We therefore hypothesized that mouse SIK3 directly regulates HDAC4. Indeed, we confirmed that SIK3 and HDAC4 form a stable complex by performing a pulldown assay. We found that the subcellular localization of SIK3 in chondrocytes in vivo was the cytoplasm. In fact, we did not find any nuclear localization signal in its sequence, and the SIK3 that was ectopically expressed in the 293FT cells was detected in the cytoplasm. By contrast, HDAC4 was detected in both the cytoplasm and the nucleus in proliferative chondrocytes, whereas it was localized in the cytoplasm in hypertrophic chondrocytes. It is also known that HDAC4 shuttles between the cytoplasm and nucleus. Considering these findings, it appears that when SIK3 is present in the cytoplasm, HDAC4 is anchored there. Consistent with this idea, we demonstrated that GFP-HDAC4, which was localized in nuclei when expressed alone, was localized in the cytoplasm when SIK3 was co-expressed in 293FT cells. Furthermore, anchoring HDAC4 to the cytoplasm by SIK3 co-expression allowed reactivation of the MEF2C repressed by HDAC4 in nuclei in vitro.

It is thought that the role of SIK3 during chondrocyte differentiation is to exclude HDAC4 from the nucleus, thereby allowing MEF2C to be transcriptionally active in the nucleus to induce progression of the chondrocyte hypertrophy program. We found that constitutively active forms of SIK3 (T163E, S494A), but not wild-type SIK3, inhibited HDAC4 activity in ATDC5 cells, suggesting the presence of other factors that are needed for SIK3 activation. Previously, LKB1 (STK11 – Mouse Genome

Informatics) was shown to be an activator of SIK3, and it phosphorylates SIK3 at Thr163 (Lizcano et al., 2004), raising the possibility that LKB1 might be a regulator of SIK3. The mild cartilage phenotype in *Col11a2-hSIK3* transgenic mice compared with that in *Mef2c* transgenic or HDAC4-deficient mice might indicate that the presence of additional factors is required for the activation of *Sik3* in chondrocytes. In the *hSIK3* transgenic growth plate, we did not see obvious changes in HDAC4 localization (data not shown) in spite of the presence of growth plate abnormalities. A possible explanation for this discrepancy is that the changes might have been too faint to be detected by immunofluorescence microscopy. It is also possible that other undefined mechanisms act downstream of SIK3, in parallel to HDAC4. *Col11a2-hSIK3* transgenic mice showed early closure of the growth plates. Growth plate disappearance has been reported in mice in which IHH (Maeda et al., 2007) and the PTH/PTHrP receptor (Hirai et al., 2011) were deleted postnatally. Because IHH and PTH/PTHrP regulate chondrocyte hypertrophy, SIK3 might be localized and controlled by these signaling molecules during the progression of chondrocyte hypertrophy. The SIK3-deficient cartilage phenotype was rescued by *Col11a2-hSIK3* transgene expression, suggesting that the impaired skeletal development in SIK3-deficient mice is primarily due to the cartilage tissue. It is also possible that changes in cholesterol metabolism and malnourishment phenotypes in the SIK3-deficient mice (T.U., Y. Itoh, O. Hatano, A. Kumagai, M. Sanosaka, T. Sasaki, S.S., J. Doi, K. Tatsumi, K. Mitamura et al., unpublished) affect chondrocyte differentiation, as cholesterol signaling stimulates chondrocyte hypertrophy (Woods et al., 2009) and because malnourishment phenotypes, including lipodystrophy, hypolipidemia and hypoglycemia, should affect skeletal growth. The SIK3-deficient bone phenotypes displayed at adulthood in this study might have occurred due to a combination of direct SIK3 disruption in chondrocytes and indirect SIK3 disruption due to metabolic changes.

Previously, PP2A was proposed as a regulator of HDAC4 by localizing it in the nucleus, thereby prohibiting chondrocyte hypertrophy (Kozhemyakina et al., 2009). However, no opposing mechanisms have been suggested. Our present findings are therefore the first to indicate that SIK3 has an antagonistic role in HDAC4 regulation during chondrogenesis. Although we did not perform an in-depth analysis of the underlying mechanism(s) of action in this study, we did observe impaired skull bone development, which occurs through membranous ossification, suggesting that SIK3 is involved in membranous ossification as well. Further studies are needed to better understand the functions of SIK3 in skeletal development, including the generation of conditional knockout mice.

Acknowledgements
We thank Dr Gen Nishimura for advice on manuscript preparation; Dr James Hsieh for providing instructions for the immunoprecipitation assay; Ms Mari Shinkawa for technical assistance; Drs Hidetatsu Outani, Hirohiko Yasui, Yoshiki Minegishi, Minoru Okada, Jun Yoshino and Takao Hirai for discussions and suggestions; and Dr Kazuyuki Itoh for support.

Funding
This study was supported in part by the Japan Science Technology Agency (JST); Core Research for Evolutional Science and Technology (CREST) (to N.T.); Ministry of Education, Culture, Sports, Science and Technology (MEXT) [Scientific Research Grant No. 21390421 to N.T.]; and the Natural Scientists and the Strategic Project to Support the Formation of Research Bases at Private Universities (to H.T.).

Competing interests statement
The authors declare no competing financial interests.

Supplementary material
Supplementary material available online at
http://dev.biologists.org/lookup/suppl/doi:10.1242/dev.072652/-/DC1

References
Akiyama, H., Chaboissier, M. C., Martin, J. F., Schedl, A. and de Crombrugghe, B. (2002). The transcription factor Sox9 has essential roles in successive steps of the chondrocyte differentiation pathway and is required for expression of Sox5 and Sox6. *Genes Dev.* **16**, 2813-2828.

Akiyama, H., Lyons, J. P., Mori-Akiyama, Y., Yang, X., Zhang, R., Zhang, Z., Deng, J. M., Taketo, M. M., Nakamura, T., Behringer, R. R. et al. (2004). Interactions between Sox9 and beta-catenin control chondrocyte differentiation. *Genes Dev.* **18**, 1072-1087.

Arnold, M. A., Kim, Y., Czubryt, M. P., Phan, D., McAnally, J., Qi, X., Shelton, J. M., Richardson, J. A., Bassel-Duby, R. and Olson, E. N. (2007). MEF2C transcription factor controls chondrocyte hypertrophy and bone development. *Dev. Cell* **12**, 377-389.

Hattori, T., Muller, C., Gebhard, S., Bauer, E., Pausch, F., Schlund, B., Bosl, M. R., Hess, A., Surmann-Schmitt, C., von der Mark, H. et al. (2010). SOX9 is a major negative regulator of cartilage vascularization, bone marrow formation and endochondral ossification. *Development* **137**, 901-911.

Hirai, T., Chagin, A. S., Kobayashi, T., Mackem, S. and Kronenberg, H. M. (2011). Parathyroid hormone/parathyroid hormone-related protein receptor signaling is required for maintenance of the growth plate in postnatal life. *Proc. Natl. Acad. Sci. USA* **108**, 191-196.

Hiramatsu, K., Sasagawa, S., Outani, H., Nakagawa, K., Yoshikawa, H. and Tsumaki, N. (2011). Generation of hyaline cartilaginous tissue from mouse adult dermal fibroblast culture by defined factors. *J. Clin. Invest.* **121**, 640-657.

Ikegami, D., Akiyama, H., Suzuki, A., Nakamura, T., Nakano, T., Yoshikawa, H. and Tsumaki, N. (2011). Sox9 sustains chondrocyte survival and hypertrophy in part through Pik3ca-Akt pathways. *Development* **138**, 1507-1519.

Karsenty, G., Kronenberg, H. M. and Settembre, C. (2009). Genetic control of bone formation. *Annu. Rev. Cell Dev. Biol.* **25**, 629-648.

Katoh, Y., Takemori, H., Horike, N., Doi, J., Muraoka, M., Min, L. and Okamoto, M. (2004). Salt-inducible kinase (SIK) isoforms: their involvement in steroidogenesis and adipogenesis. *Mol. Cell. Endocrinol.* **217**, 109-112.

Katoh, Y., Takemori, H., Lin, X. Z., Tamura, M., Muraoka, M., Satoh, T., Tsuchiya, Y., Min, L., Doi, J., Miyauchi, A. et al. (2006). Silencing the constitutive active transcription factor CREB by the LKB1-SIK signaling cascade. *FEBS J.* **273**, 2730-2748.

Komori, T., Yagi, H., Nomura, S., Yamaguchi, A., Sasaki, K., Deguchi, K., Shimizu, Y., Bronson, R. T., Gao, Y. H., Inada, M. et al. (1997). Targeted disruption of Cbfa1 results in a complete lack of bone formation owing to maturational arrest of osteoblasts. *Cell* **89**, 755-764.

Kozhemyakina, E., Cohen, T., Yao, T. P. and Lassar, A. B. (2009). Parathyroid hormone-related peptide represses chondrocyte hypertrophy through a protein phosphatase 2A/histone deacetylase 4/MEF2 pathway. *Mol. Cell. Biol.* **29**, 5751-5762.

Lefebvre, V. and Smits, P. (2005). Transcriptional control of chondrocyte fate and differentiation. *Birth Defects Res. C Embryo Today* **75**, 200-212.

Lizcano, J. M., Goransson, O., Toth, R., Deak, M., Morrice, N. A., Boudeau, J., Hawley, S. A., Udd, L., Makela, T. P., Hardie, D. G. et al. (2004). LKB1 is a master kinase that activates 13 kinases of the AMPK subfamily, including MARK/PAR-1. *EMBO J.* **23**, 833-843.

Maeda, Y., Nakamura, E., Nguyen, M. T., Suva, L. J., Swain, F. L., Razzaque, M. S., Mackem, S. and Lanske, B. (2007). Indian Hedgehog produced by postnatal chondrocytes is essential for maintaining a growth plate and trabecular bone. *Proc. Natl. Acad. Sci. USA* **104**, 6382-6387.

Mitchell, P. G., Magna, H. A., Reeves, L. M., Lopresti-Morrow, L. L., Yocum, S. A., Rosner, P. J., Geoghegan, K. F. and Hambor, J. E. (1996). Cloning, expression, and type II collagenolytic activity of matrix metalloproteinase-13 from human osteoarthritic cartilage. *J. Clin. Invest.* **97**, 761-768.

Murai, J., Ikegami, D., Okamoto, M., Yoshikawa, H. and Tsumaki, N. (2008). Insulation of the ubiquitous Rxrb promoter from the cartilage-specific adjacent gene, Col11a2. *J. Biol. Chem.* **283**, 27677-27687.

Nakashima, K., Zhou, X., Kunkel, G., Zhang, Z., Deng, J. M., Behringer, R. R. and de Crombrugghe, B. (2002). The novel zinc finger-containing transcription factor osterix is required for osteoblast differentiation and bone formation. *Cell* **108**, 17-29.

Ng, L. J., Wheatley, S., Muscat, G. E., Conway-Campbell, J., Bowles, J., Wright, E., Bell, D. M., Tam, P. P., Cheah, K. S. and Koopman, P. (1997). SOX9 binds DNA, activates transcription, and coexpresses with type II collagen during chondrogenesis in the mouse. *Dev. Biol.* **183**, 108-121.

Olsen, B. R., Reginato, A. M. and Wang, W. (2000). Bone development. *Annu. Rev. Cell Dev. Biol.* **16**, 191-220.

Takeda, S., Bonnamy, J. P., Owen, M. J., Ducy, P. and Karsenty, G. (2001). Continuous expression of Cbfa1 in nonhypertrophic chondrocytes uncovers its ability to induce hypertrophic chondrocyte differentiation and partially rescues Cbfa1-deficient mice. *Genes Dev.* **15**, 467-481.

Takeda, S., Chen, D. Y., Westergard, T. D., Fisher, J. K., Rubens, J. A., Sasagawa, S., Kan, J. T., Korsmeyer, S. J., Cheng, E. H. and Hsieh, J. J. (2006). Proteolysis of MLL family proteins is essential for taspase1-orchestrated cell cycle progression. *Genes Dev.* **20**, 2397-2409.

Takemori, H., Katoh Hashimoto, Y., Nakae, J., Olson, E. N. and Okamoto, M. (2009). Inactivation of HDAC5 by SIK1 in AICAR-treated C2C12 myoblasts. *Endocrine J.* **56**, 121-130.

Tsumaki, N., Kimura, T., Matsui, Y., Nakata, K. and Ochi, T. (1996). Separable cis-regulatory elements that contribute to tissue- and site-specific alpha 2(XI) collagen gene expression in the embryonic mouse cartilage. *J. Cell Biol.* **134**, 1573-1582.

van der Linden, A. M., Nolan, K. M. and Sengupta, P. (2007). KIN-29 SIK regulates chemoreceptor gene expression via an MEF2 transcription factor and a class II HDAC. *EMBO J.* **26**, 358-370.

Vega, R. B., Matsuda, K., Oh, J., Barbosa, A. C., Yang, X., Meadows, E., McAnally, J., Pomajzl, C., Shelton, J. M., Richardson, J. A. et al. (2004). Histone deacetylase 4 controls chondrocyte hypertrophy during skeletogenesis. *Cell* **119**, 555-566.

Wang, B., Moya, N., Niessen, S., Hoover, H., Mihaylova, M. M., Shaw, R. J., Yates, J. R., 3rd, Fischer, W. H., Thomas, J. B. and Montminy, M. (2011). A hormone-dependent module regulating energy balance. *Cell* **145**, 596-606.

Woods, A., James, C. G., Wang, G., Dupuis, H. and Beier, F. (2009). Control of chondrocyte gene expression by actin dynamics: a novel role of cholesterol/Ror-alpha signalling in endochondral bone growth. *J. Cell. Mol. Med.* **13**, 3497-3516.

Zhao, Q., Eberspaecher, H., Lefebvre, V. and De Crombrugghe, B. (1997). Parallel expression of Sox9 and Col2a1 in cells undergoing chondrogenesis. *Dev. Dyn.* **209**, 377-386.

Development 138, 1507-1519 (2011) doi:10.1242/dev.057802

Sox9 sustains chondrocyte survival and hypertrophy in part through Pik3ca-Akt pathways

Daisuke Ikegami[1,2], Haruhiko Akiyama[3], Akira Suzuki[4,5], Takashi Nakamura[3], Toru Nakano[6], Hideki Yoshikawa[2] and Noriyuki Tsumaki[1,2,7,*]

SUMMARY

During endochondral bone formation, Sox9 expression starts in mesenchymal progenitors, continues in the round and flat chondrocyte stages at high levels, and ceases just prior to the hypertrophic chondrocyte stage. Sox9 is important in mesenchymal progenitors for their differentiation into chondrocytes, but its functions post-differentiation have not been determined. To investigate Sox9 function in chondrocytes, we deleted mouse *Sox9* at two different steps after chondrocyte differentiation. Sox9 inactivation in round chondrocytes resulted in a loss of *Col2a1* expression and in apoptosis. Sox9 inactivation in flat chondrocytes caused immediate terminal maturation without hypertrophy and with excessive apoptosis. Inactivation of Sox9 in the last few cell layers resulted in the absence of *Col10a1* expression, suggesting that continued expression of Sox9 just prior to hypertrophy is necessary for chondrocyte hypertrophy. SOX9 knockdown also caused apoptosis of human chondrosarcoma SW1353 cells. These phenotypes were associated with reduced Akt phosphorylation. Forced phosphorylation of Akt by *Pten* inactivation partially restored *Col10a1* expression and cell survival in $Sox9^{floxdel/floxdel}$ mouse chondrocytes, suggesting that phosphorylated Akt mediates chondrocyte survival and hypertrophy induced by Sox9. When the molecular mechanism of Sox9-induced Akt phosphorylation was examined, we found that expression of the PI3K subunit Pik3ca (p110α) was decreased in $Sox9^{floxdel/floxdel}$ mouse chondrocytes. Sox9 binds to the promoter and enhances the transcriptional activities of *Pik3ca*. Thus, continued expression of Sox9 in differentiated chondrocytes is essential for subsequent hypertrophy and sustains chondrocyte-specific survival mechanisms by binding to the *Pik3ca* promoter, inducing Akt phosphorylation.

KEY WORDS: Sox9, Chondrocytes, Collagen, Conditional knockout, Transcriptional regulation, Mouse

INTRODUCTION

During development, the limb skeleton is created through endochondral bone formation. Mesenchymal cells initially undergo condensation, which is followed by the differentiation of prechondrogenic cells within these condensations into round chondrocytes, which proliferate and produce cartilage extracellular matrix to form cartilage primordia. Proliferating chondrocytes in the central region of the cartilage then exit the cell cycle and differentiate into prehypertrophic and, subsequently, hypertrophic chondrocytes. The proliferating chondrocytes closest to the prehypertrophic chondrocytes flatten out and form orderly columns of flat chondrocytes that are still proliferating. Finally, hypertrophic chondrocytes progress to terminal maturation to express matrix metalloproteinase 13 (Mmp13). Terminally mature chondrocytes undergo apoptosis. Blood vessels along with osteoblasts, osteoclasts and hematopoietic cells then invade and form primary ossification centers (Lefebvre and Smits, 2005). Cartilage at both ends of each skeletal component remains as articular cartilage and sustains joint movement.

Sox9 is a member of the SOX (Sry-related high mobility group box) family of transcription factors that share the high mobility group (HMG) DNA-binding motif with the mammalian testis-determining factor Sry. Heterozygous mutations in the human *SOX9* gene cause the skeletal malformation syndrome campomelic dysplasia (Foster et al., 1994; Wagner et al., 1994). Sox9 is expressed in progenitor cells in various organs (Akiyama et al., 2005), including chondroprogenitors, osteoprogenitors and preadipocytes (Wang and Sul, 2009), but is not expressed in most differentiated somatic cells such as osteoblasts and adipocytes (Wang and Sul, 2009), with the exception of chondrocytes. During endochondral bone formation, Sox9 expression starts in mesenchymal progenitor cells. Sox9 remains highly expressed in chondrocytes, and its expression ceases in prehypertrophic chondrocytes (Ng et al., 1997; Zhao et al., 1997). SOX9 expression continues in articular cartilage and decreases in osteoarthritic cartilage, a major cartilage disease caused by degeneration (Brew et al., 2010). That Sox9 plays a crucial role in mesenchymal progenitor cells has been established by analysis of *Sox9* knockout chimeras and conditional knockout mice. In mouse chimeras, $Sox9^{-/-}$ cells are excluded from cartilage primordia throughout embryonic development (Bi et al., 1999). Furthermore, mesenchymal condensation and subsequent cartilage formation are absent in the limbs of *Prx1-Cre;* $Sox9^{flox/flox}$ conditional knockout mice, in which the *Sox9* gene is inactivated in early mesenchymal limb bud cells before mesenchymal condensation occurs (Akiyama et al., 2002). In addition, the cartilage is very hypoplastic in *Col2a1-Cre;* $Sox9^{flox/flox}$ conditional knockout mice, in which Sox9

[1]Departments of Bone and Cartilage Biology, Osaka University Graduate School of Medicine, 2-2 Yamadaoka, Suita, Osaka 565-0871, Japan. [2]Department of Orthopaedic Surgery, Osaka University Graduate School of Medicine, 2-2 Yamadaoka, Suita, Osaka 565-0871, Japan. [3]Department of Orthopaedics, Graduate School of Medicine, Kyoto University, 54 Kawahara-cho, Shogoin, Sakyo-ku, Kyoto 606-8507, Japan. [4]Division of Cancer Genetics, Medical Institute of Bioregulation, Kyushu University, Fukuoka 812-8582, Japan. [5]Global Center of Excellence (COE) Program, Akita University Graduate School of Medicine, Akita 010-8543, Japan. [6]Department of Pathology, Medical School and Graduate School of Frontier Biosciences, Osaka University, Suita, Osaka 565-0871, Japan. [7]Japan Science and Technology Agency, CREST, Tokyo 102-0075, Japan.

*Author for correspondence (ntsumaki@dbcb.med.osaka-u.ac.jp)

Accepted 14 January 2011

expression is lost in condensed mesenchymal cells before differentiation into chondrocytes. In *Col2a1-Cre; Sox9$^{flox/flox}$* mice, *Sox9$^{floxdel/floxdel}$* cells remain as condensed mesenchymal cells and do not differentiate into chondrocytes (Akiyama et al., 2002).

The function of Sox9 expression post-differentiation into chondrocytes has not been determined. The functions of Sox9 in chondrocytes cannot be determined from previously reported chimeras or conditional knockout mice because they lack chondrocytes. Emerging evidence suggests that Sox9 inhibits chondrocyte hypertrophy; *Sox9$^{+/-}$* embryos show premature mineralization of cartilage and expanded hypertrophic zones (Bi et al., 2001). Mice that overexpress *Sox9* under the control of *Col2a1* regulatory elements exhibit delayed cartilage mineralization (Akiyama et al., 2004). In these genetically modified mice, however, the nature of the chondrocytes and matrix properties are altered before differentiation into chondrocytes owing to the manipulation of Sox9 expression from the stage of mesenchymal progenitor cells. A recent study has shown that misexpression of Sox9 in hypertrophic chondrocytes results in a lack of bone marrow, and that Sox9 is a major negative regulator of cartilage vascularization (Hattori et al., 2010).

We recently generated two types of transgenic mice in which Cre is expressed at different steps during chondrocyte differentiation (Iwai et al., 2008). In *11Enh-Cre* transgenic mice, Cre recombinase activities are controlled by the *Col11a2* promoter and enhancer and begin during the round chondrocyte stage. *11Enh-Cre* directs recombination at a later stage (both developmental and within the chondrocyte differentiation pathway) than *Col2a1-Cre*. Cre recombinase activities in *11Prom-Cre* transgenic mice are controlled by the *Col11a2* promoter alone and begin in the flat chondrocyte stage. In the present study, we examined the function of Sox9 in chondrocytes by generating *11Enh-Cre; Sox9$^{flox/flox}$* and *11Prom-Cre; Sox9$^{flox/flox}$* conditional knockout mice.

MATERIALS AND METHODS

Animals and genotyping

To generate *Sox9* conditional knockout mice, *11Enh-Cre* transgenic mice, *11Prom-Cre* transgenic mice (Iwai et al., 2008) and *Sox9$^{flox/flox}$* mice (Akiyama et al., 2002) were prepared and mated. To generate *Sox9; Pten* double conditional knockout mice, *Pten$^{flox/flox}$* mice (Suzuki et al., 2001) were prepared. For genotyping, genomic DNA was isolated from tail tips or embryonic skin and subjected to PCR analysis according to the methods previously described for the *Cre* transgene (Iwai et al., 2008), *Sox9* allele (Akiyama et al., 2002) and *Pten* allele (Suzuki et al., 2001).

Real-time RT-PCR

Total RNA was extracted using the RNeasy Mini Kit (Qiagen). Total RNAs were digested with DNase to eliminate any contaminating genomic DNA. PCR amplification was with SYBR Premix ExTaq (Takara) on a 7900HT real-time PCR system (Applied Biosystems). RNA expression levels were normalized to that of *Gapdh*. The primers used are listed in Table S1 in the supplementary material.

Staining of the skeleton

Embryos were dissected, fixed in 100% ethanol overnight, and then stained with Alcian Blue followed by Alizarin Red S solution according to standard protocols (Peters, 1977).

Histological analysis

Embryos were dissected under a stereomicroscope, fixed in 4% paraformaldehyde, processed and embedded in paraffin. For immunohistochemistry, sections were incubated with primary antibodies (Table 1). Immune complexes were detected using secondary antibodies conjugated to Alexa Fluor 488 (Table 1). RNA in situ hybridization was performed using ^{35}S-labeled antisense riboprobes as previously described (Pelton et al., 1990) or using a DIG RNA labeling kit (Boehringer Mannheim, Indianapolis, IN, USA) according to the manufacturer's instructions. In situ hybridization and immunohistochemistry were performed at least three times for each analysis.

BrdU staining

Pregnant mice were intraperitoneally injected with BrdU labeling reagent (10 μl/g body weight; Zymed Laboratories, South San Francisco, CA, USA). Two hours later, the mice were sacrificed and embryos were dissected and sectioned. Incorporated BrdU was detected using a BrdU staining kit (Zymed Laboratories) to distinguish actively proliferating cells. The average number of BrdU-positive cells among total cells (± s.d.) was calculated.

TUNEL assay

TUNEL assays were performed on semi-serial sections using the DeadEnd Fluorometric TUNEL System (Promega) according to the manufacturer's protocol.

Microscopy

Images were acquired on an inverted microscope (Eclipse Ti, Nikon) equipped with cameras (DS-Fi1, Nikon; C4742-80-12AG, Hamamatsu Photonics) and NIS Elements software (Nikon).

Table 1. Antibodies used in western blots and immunohistochemistry (IHC)

Antibody	Source (Cat. No.)	Dilution	
		Western	IHC
Anti-type I collagen	Abcam (ab34710)	–	1/1000
Anti-Sox9	Santa Cruz (sc-20095)	1/200	1/400
Anti-cleaved caspase 3	Cell Signaling (#9661)	–	1/100
Anti-Pten	Cell Signaling (#9559)	–	1/200
Anti-Pik3ca (p110α)	Cell Signaling (#4249)	1/1000	1/400
Anti-Pik3cb (p110β)	Cell Signaling (#3011)	1/1000	1/100
Anti-Pik3r1 and Pik3r2 (p85)	Cell Signaling (#4257)	1/1000	1/100
Anti-phospho-Akt	Cell Signaling (#4060)	1/1000	1/50
Anti-Akt	Cell Signaling (#4685)	1/1000	1/50
Anti-phospho-ATF2	Cell Signaling (#9221)	1/1000	1/100
Anti-ATF2	Cell Signaling (#9226)	1/1000	–
Anti-phospho-SAPK/JNK	Cell Signaling (#9251)	1/1000	1/100
Anti-phospho-p38 MAP kinase	Cell Signaling (#9211)	1/1000	1/100
Anti-p38 MAP kinase (MAPK14)	Cell Signaling (#9212)	1/1000	–
Anti-phospho-ERK1/2	Cell Signaling (#9101)	1/1000	–
Anti-ERK1/2 (MAPK3/1)	Cell Signaling (#4695)	1/1000	–
Anti-β-actin	Cell Signaling (#4967)	1/1000	–
Alexa Fluor 488 goat anti-rabbit	Invitrogen (A11008)	–	1/2000

Western blot analysis
Cell lysates were subjected to SDS-PAGE, electroblotted and immunostained with the antibodies listed in Table 1. Immunoblots were performed at least three times for each analysis.

Cell lines and cell culture
SW1353 (ATCC #HTB94), HeLa (Riken #RBC0007) and Saos2 (Riken #RCB0428) cells were cultured in Dulbecco's Modified Eagle's Medium (DMEM) supplemented with 10% fetal bovine serum (FBS) and 1% streptomycin/penicillin. ATDC5 cells were maintained at 20-80% confluency as described previously (Shukunami et al., 1996). For SOX9 overexpression experiments, SW1353 cells were transfected with the plasmid CMV promoter-SOX9 using Amaxa nucleofection technologies. Cells were harvested for real-time RT-PCR and immunoblot analysis 24 hours after transfection.

Knockdown of SOX9 via RNA interference
Amaxa nucleofection technology was used to transfect 1×10^6 SW1353, HeLa or Saos2 cells with 200 nM negative control siRNA (Stealth RNAi Negative Control Medium GC Duplex #2, 12935-112, Invitrogen) or SOX9-a, SOX9-b or SOX9-c siRNAs (Invitrogen Stealth RNAi; siRNA target sequences are listed in Table S2 in the supplementary material).

Six hours after transfection, cell lysates were collected for immunoblot analysis. For morphological evaluation, 1×10^6 cells were seeded into 6-well plates and 6 hours after transfection cells were stained with Hoechst 33342 (Dojindo Laboratories, Japan). Caspase 3/7 activities were measured 6 hours after transfection using the Caspase-Glo3/7 Assay Kit (Promega) according to the manufacturer's instructions. Six hours after transfection, the level of apoptosis was determined using the Cell Death Detection ELISA^{PLUS} Kit (Roche Applied Science).

Luciferase reporter assay
Various lengths of human *PIK3CA* promoter sequence (Hui et al., 2008) were prepared. Mutations were introduced using the GeneTailor Site-Directed Mutagenesis System (Invitrogen). Fragments were inserted into the pGL3-basic vector (Promega). Undifferentiated ATDC5 cells and SW1353 cells were co-transfected with 20 ng reporter construct, 10 ng phRL-TK (Promega) and a total of 200 ng SOX9 expression vector and mock vector using FuGENE (Roche). Cell lysates were collected 48 hours after transfection. Photinus luciferase activity levels were normalized to those of Renilla luciferase (phRL-TK).

Chromatin immunoprecipitation (ChIP) assay
A ChIP assay kit (Upstate #17-295) was used according to the manufacturer's protocol. The purified DNA was used as a template in PCR assays. The primers are listed in Table S3 in the supplementary material.

Statistical analyses
Data are shown as averages with standard deviations. Student's *t*-test was used to compare data. $P<0.05$ was considered statistically significant.

RESULTS

Generation of *11Enh-Cre; Sox9$^{flox/flox}$* conditional knockout mice
We initially intercrossed *11Enh-Cre* mice (Iwai et al., 2008) with *Sox9$^{flox/flox}$* mice (Akiyama et al., 2002). *Sox9$^{flox/+}$* heterozygotes that harbor *11Enh-Cre* were recovered with the expected Mendelian frequency (see Fig. S1A in the supplementary material); these mice were fertile and developed dwarfism (see Fig. S1B in the supplementary material). Eighty-five percent of *11Enh-Cre; Sox9$^{flox/+}$* mice were viable beyond 6 months of age (see Fig. S1C in the supplementary material), suggesting that these mice have a much milder phenotype than *Col2a1-Cre; Sox9$^{flox/+}$* mice, which have a 95% death rate by 10 days of age (Akiyama et al., 2002).

We then intercrossed *11Enh-Cre; Sox9$^{flox/+}$* mice with *Sox9$^{flox/flox}$* mice (see Fig. S1D in the supplementary material). The cartilage and bone of *11Enh-Cre; Sox9$^{flox/flox}$* embryos at 16.5 days post-coitum (dpc) were very hypoplastic, whereas the calvarium, which undergoes membranous ossification and is formed without cartilage templates, appeared to be well formed (see Fig. S1E-G in the supplementary material).

11Enh-Cre; Sox9$^{flox/flox}$ mice start to lose Sox9 expression in round chondrocytes, resulting in apoptosis
Histological analysis showed that *11Enh-Cre; Sox9$^{flox/flox}$* conditional knockout embryos exhibited normal mesenchymal condensation with normal Sox9 expression patterns in paws at 12.5 dpc (Fig. 1A). At 12.5 dpc, cells in the central region of mesenchymal condensation at the humerus differentiated into round chondrocytes, as indicated by round or polygonal cell morphologies and slight staining of the surrounding matrix with Safranin O in control *Sox9$^{flox/+}$* embryos (Fig. 1B, left column). Round chondrocytes in the central region of condensation in *11Enh-Cre; Sox9$^{flox/flox}$* humerus showed decreased staining of the matrix with Safranin O and lost Sox9 expression (Fig. 1B, right column). These results suggest that *11Enh-Cre* initiated the direct recombination of floxed *Sox9* genes in round chondrocytes. At 13.5 dpc, the primordial cartilage of control *Sox9$^{flox/+}$* mouse humerus was formed, as indicated by Safranin O staining (Fig. 1C). Immunohistochemistry with anti-Sox9 antibodies showed that proliferative chondrocytes in cartilage expressed Sox9. By contrast, primordial cartilage in *11Enh-Cre; Sox9$^{flox/flox}$* humerus was disorganized at 13.5 dpc, with weak Safranin O staining intensities, and the chondrocytes in the central region of cartilage had lost Sox9 expression. Cells in the periphery of the primordial cartilage still expressed Sox9. *Col2a1* expression was lost in accordance with the loss of Sox9. This in vivo result supports the notion that Sox9 is needed for the maintenance of *Col2a1* transcription in chondrocytes. Hypertrophic chondrocytes were absent and *Col10a1* expression was lost. At 14.5 dpc, *11Enh-Cre; Sox9$^{flox/flox}$* humerus showed only a small amount of cartilage, which was disorganized and lacked hypertrophic chondrocytes (Fig. 1D). *Ihh* expression was almost completely lost and expression of *Col10a1* and *Mmp13* was lost. Runx2 expression was maintained in bone collars. These results suggest that *Sox9* deletion in round chondrocytes abolishes the subsequent differentiation of chondrocytes.

Together with an existing report that the loss of Sox9 is associated with apoptosis in neural crest cells (Cheung et al., 2005), the presence of just a small amount of disorganized cartilage, despite the initial mesenchymal condensation, raised the possibility that chondrocytes underwent apoptosis. We found that cells were TUNEL negative and did not show immunoreactivity for cleaved caspase 3 in either *11Enh-Cre; Sox9$^{flox/flox}$* or *Sox9$^{flox/+}$* humerus at 12.5 dpc (see Fig. S2A in the supplementary material). Cells in the epiphyseal region within the disorganized cartilage in *11Enh-Cre; Sox9$^{flox/flox}$* humerus showed TUNEL staining and immunoreactivity for cleaved caspase 3, whereas chondrocytes in the control *Sox9$^{flox/+}$* humerus did not at 13.5 dpc (Fig. 1E). As for positive controls, TUNEL-positive cells were detected in the interdigital regions of paws of both control *Sox9$^{flox/+}$* and *11Enh-Cre; Sox9$^{flox/flox}$* embryos at 13.5 dpc (see Fig. S2B in the supplementary material). These results suggest that epiphyseal chondrocytes undergo apoptosis ~1 day after deletion of *Sox9* in round chondrocytes.

Disorganized primary ossification centers were formed in *11Enh-Cre; Sox9$^{flox/flox}$* humerus at 15.5 dpc (see Fig. S2C in the supplementary material). *Col2a1* expression was almost completely

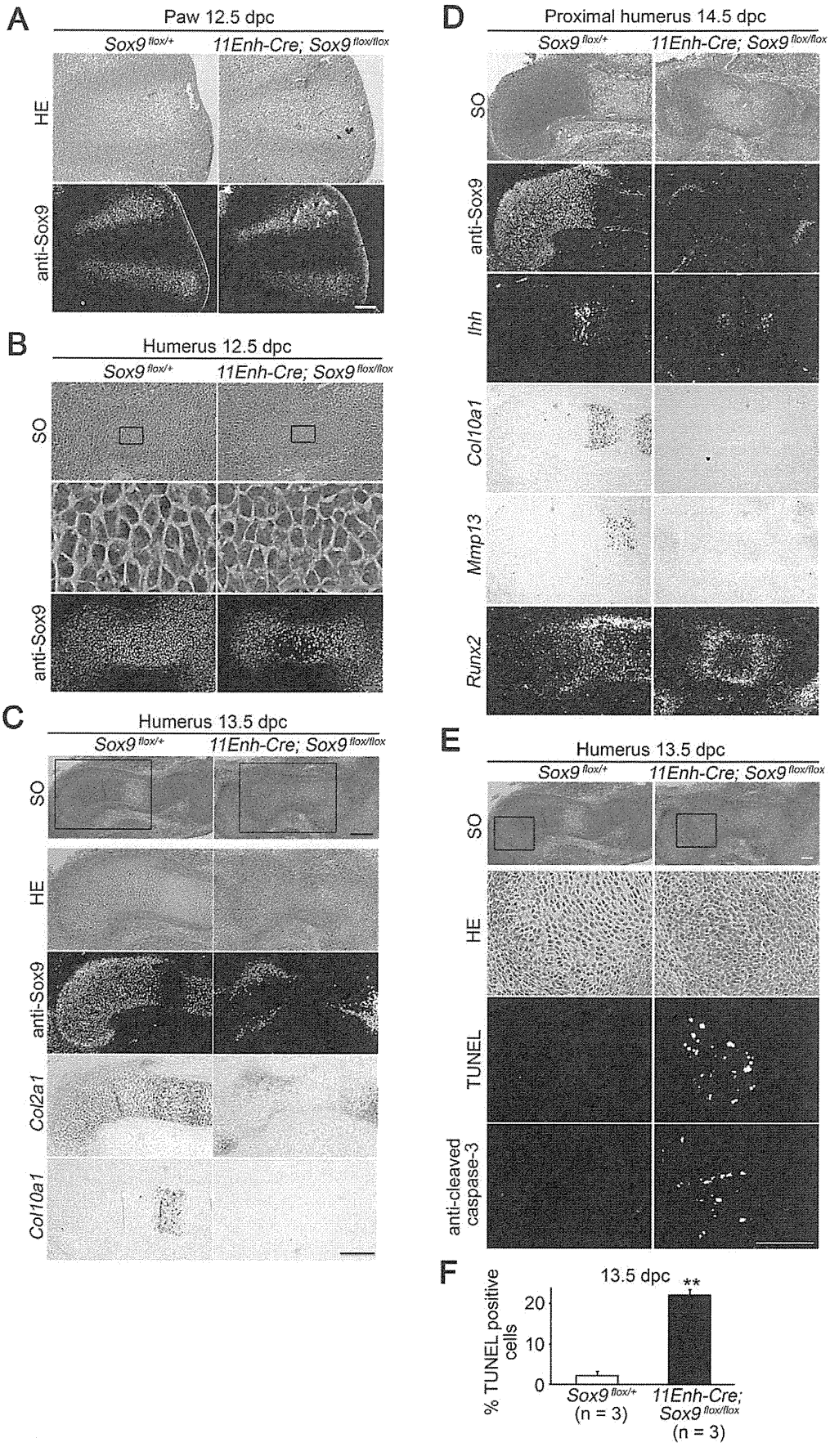

Fig. 1. Loss of Sox9 in round chondrocytes results in apoptosis in *11Enh-Cre; Sox9$^{flox/flox}$* mice. Semi-serial sections were stained with Hematoxylin and Eosin (HE) or Safranin O-Fast Green-Iron Hematoxylin (SO), immunostained with anti-Sox9 or anti-cleaved caspase 3 antibodies, hybridized with *Col2a1*, *Col10a1*, *Ihh*, *Mmp13* or *Runx2* cRNA probes, or subjected to the TUNEL assay, as indicated. (**A**) *11Enh-Cre; Sox9$^{flox/flox}$* forelimb paws at 12.5 dpc. (**B**) *11Enh-Cre; Sox9$^{flox/flox}$* humerus at 12.5 dpc. Higher magnifications of the boxed regions are shown in the middle row. (**C**) *11Enh-Cre; Sox9$^{flox/flox}$* proximal humerus at 13.5 dpc. Higher magnifications of the boxed regions are shown in rows 2-5. Most *11Enh-Cre; Sox9$^{flox/flox}$* chondrocytes did not express Sox9, indicating that their *Sox9* gene was deleted (*Sox9$^{floxdel/floxdel}$* chondrocytes). (**D**) *11Enh-Cre; Sox9$^{flox/flox}$* proximal humerus at 14.5 dpc. (**E**) *11Enh-Cre; Sox9$^{flox/flox}$* proximal humeral cartilage at 13.5 dpc. Higher magnifications of the boxed regions are shown in rows 2-4. (**F**) The percentage of TUNEL-positive cells among the total cell number was significantly increased in *11Enh-Cre; Sox9$^{flox/flox}$* versus *Sox9$^{flox/+}$* humerus (**, $P<0.01$). Data are mean + s.d. Scale bars: 100 μm in A,E; 50 μm in B; 200 μm in C,D.

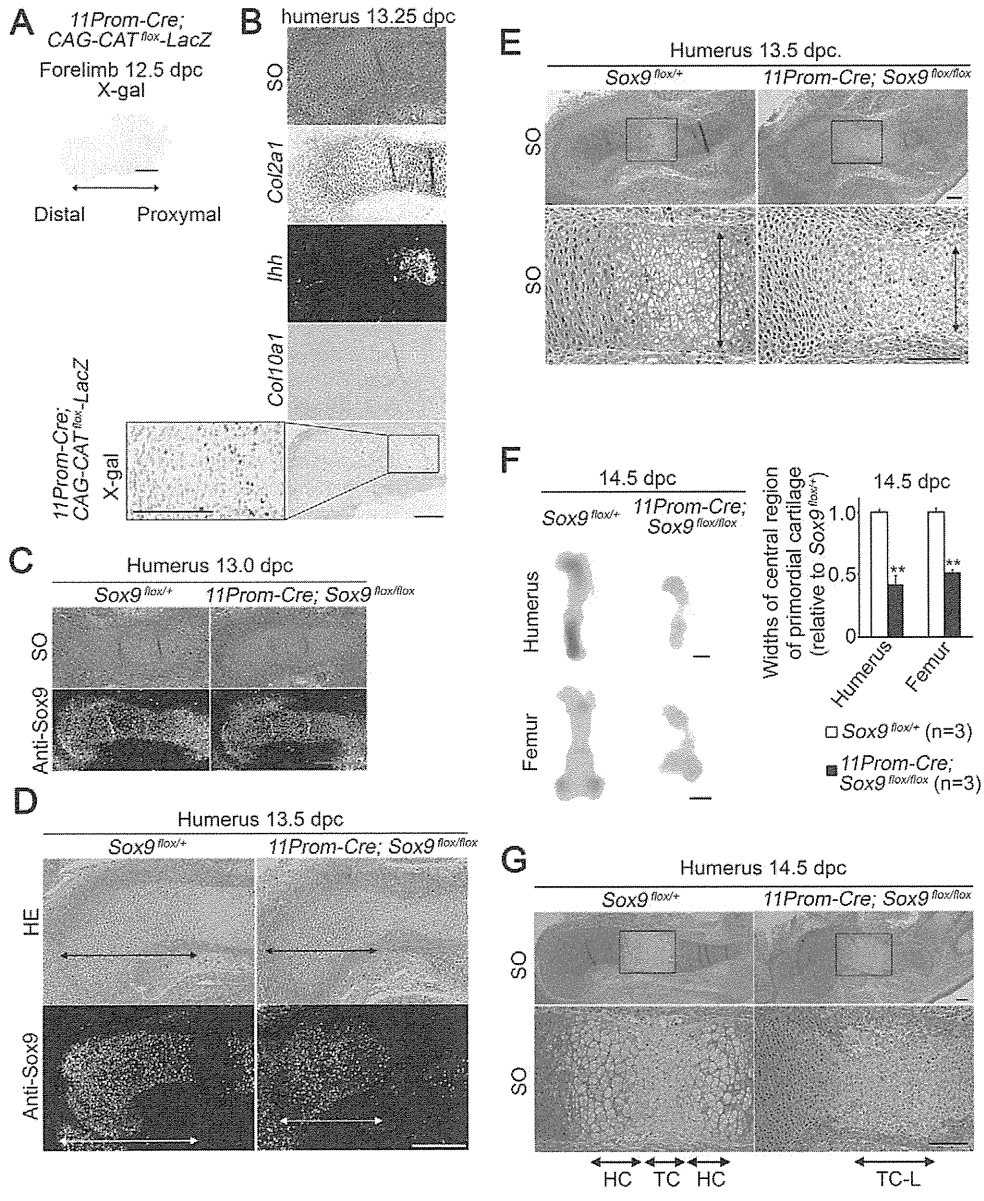

Fig. 2. Premature shutdown of Sox9 expression in flat chondrocytes results in a loss of hypertrophic chondrocytes in *11Prom-Cre; Sox9$^{flox/flox}$* mice. Semi-serial sections were stained with HE, SO or for *lacZ* expression (X-gal), immunostained with anti-Sox9, or hybridized with *Col2a1*, *Col10a1* or *Ihh* cRNA probes as indicated. (**A**,**B**) Cre-mediated recombination patterns of *11Prom-Cre* analyzed by mating with *CAG promoter-flox-CAT-flox-lacZ* transgenic tester mice. *lacZ* activity was detected in several layers of chondrocytes in the humerus at 13.25 dpc, which is when prehypertrophy starts at the center of the primordial cartilage as indicated by *Ihh* expression. (**C**) *11Prom-Cre; Sox9$^{flox/flox}$* versus *Sox9$^{flox/+}$* humerus at 13.0 dpc. (**D**) *11Prom-Cre; Sox9$^{flox/flox}$* humerus at 13.5 dpc shows a shorter zone (arrows) of proliferative chondrocytes that expressed Sox9 than the *Sox9$^{flox/+}$* control. (**E**) The width of the central region of primordial cartilage in *11Prom-Cre; Sox9$^{flox/flox}$* humerus at 13.5 dpc was decreased. Higher magnifications of the boxed regions are shown beneath. (**F**) Cartilaginous skeletons were stained with Alcian Blue. Data are mean ± s.d.; **, $P<0.01$. (**G**) The central region of the control *Sox9$^{flox/+}$* humerus consisted of a terminally mature chondrocyte zone (TC) flanked by hypertrophic chondrocyte zones (HC). The central region of the *11Prom-Cre; Sox9$^{flox/flox}$* humerus lacked hypertrophic chondrocyte zones and contained cells that resembled terminally mature chondrocytes (TC-L). Higher magnifications of the boxed regions are shown beneath. Scale bars: 200 μm in A-D,F; 100 μm in E,G.

lost and expression of *Ihh* and *Col10a1* was lost. Expression of *Mmp13* was lost in chondrocytes but maintained in the primary ossification center. Bone in the primary ossification center could have been formed by endochondral ossification through abnormal chondrocytes that survived after *Sox9* deletion or by membranous ossification from the bone collar.

Generation of *11Prom-Cre; Sox9$^{flox/flox}$* conditional knockout mice

We intercrossed *11Prom-Cre* mice (Iwai et al., 2008) with *Sox9$^{flox/flox}$* mice (Akiyama et al., 2002) to examine Sox9 function in chondrocytes at a later stage of differentiation. *11Prom-Cre; Sox9$^{flox/+}$* mice were recovered with the expected Mendelian frequency (see Fig. S3A in the supplementary material), developed normally and showed similar crown-rump lengths as control *Sox9$^{flox/+}$* mice 3 weeks after birth (see Fig. S3B in the supplementary material). *11Prom-Cre; Sox9$^{flox/flox}$* embryos were recovered with the expected Mendelian frequency from 12.5-16.5 dpc (see Fig. S3C in the supplementary material). The skeleton was very hypoplastic, whereas the calvarium appeared to be well formed (see Fig. S3D-G in the supplementary material). The cartilage of the limb buds and vertebral bodies was very hypoplastic.

11Prom-Cre; Sox9$^{flox/flox}$ mice start to lose Sox9 expression in flat chondrocytes closest to prehypertrophic chondrocytes

Cre-mediated recombination patterns of *11Prom-Cre* were analyzed by mating *11Prom-Cre* transgenic mice with *CAG promoter-flox-CAT-flox-lacZ* transgenic tester mice (Sakai and Miyazaki, 1997). No recombination was detected in limbs at 12.5 dpc (Fig. 2A). *lacZ* activity was detected in several layers of chondrocytes in the humerus at 13.25 dpc, which is when prehypertrophy starts at the center of the primordial cartilage. In situ hybridization analysis of sections from different samples at the same stage of 13.25 dpc showed that recombination started to occur in *Ihh*-expressing cells

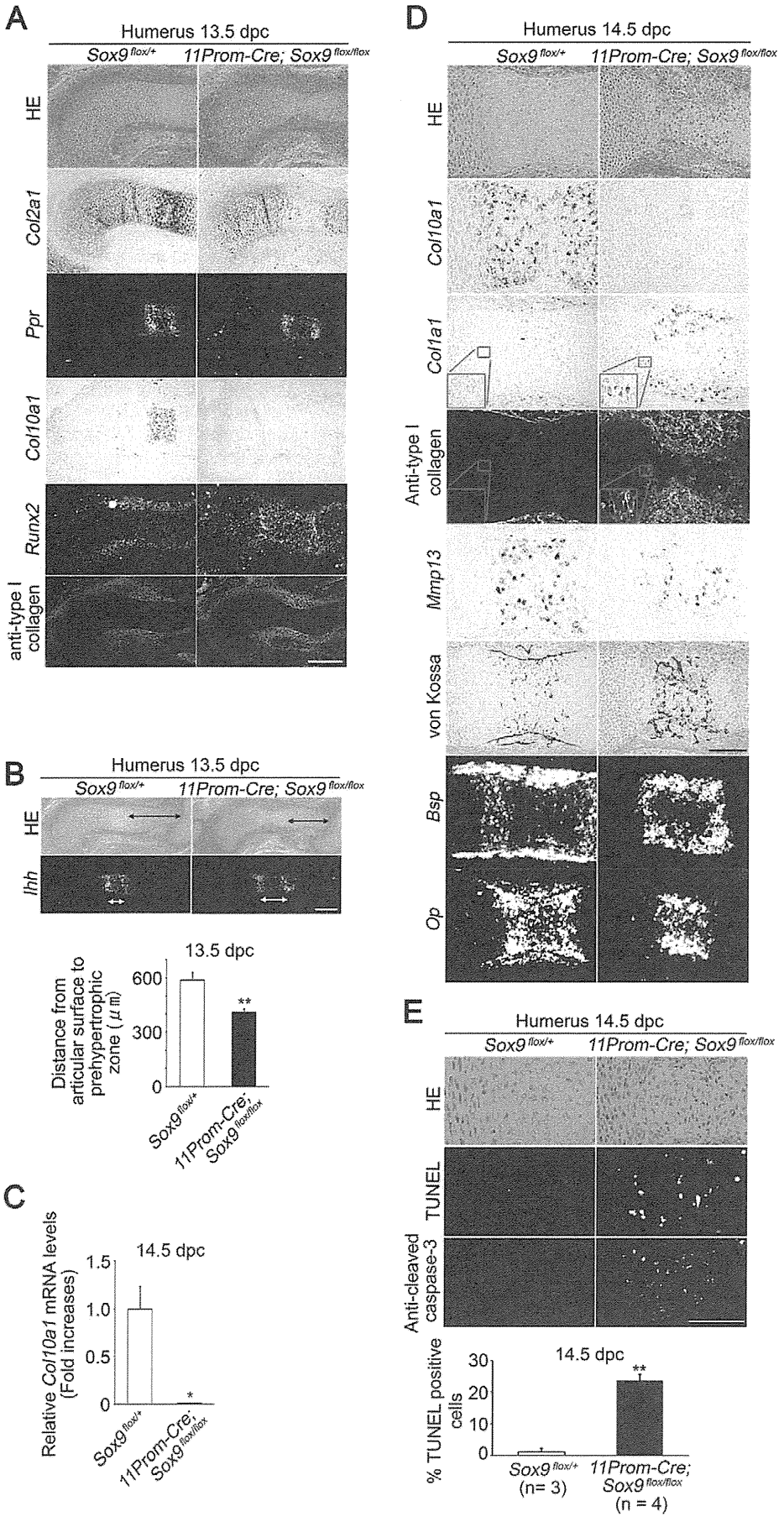

Fig. 3. Shift of prehypertrophy towards articular ends, absence of hypertrophy, and enhanced apoptosis in chondrocytes of *11Prom-Cre; Sox9$^{flox/flox}$* mice. Semi-serial sections were stained with HE or von Kossa, immunostained with anti-cleaved caspase 3 or type I collagen antibodies, hybridized with the indicated cRNA probes, or subjected to the TUNEL assay, as labeled. (**A**) Proximal humerus at 13.5 dpc. (**B**) Humerus at 13.5 dpc. n=3. (**C**) Real-time RT-PCR analysis of *Col10a1* expression in the humerus. The control *Sox9$^{flox/+}$* expression level was set at 1. n=3. (**D**) Semi-serial sections of the central region of humeral cartilage at 14.5 dpc. (**E**) Semi-serial sections of the central region of humeral cartilage at 14.5 dpc. The percentage of TUNEL-positive cells among the total cell number was significantly increased in *11Prom-Cre; Sox9$^{flox/flox}$* versus *Sox9$^{flox/+}$* humerus. Data (B,C,E) are mean + s.d. *, P<0.05; **, P<0.01. Scale bars: 200 μm in A,B; 100 μm in D,E.

(Fig. 2B). At later stages, cells closest to the prehypertrophic chondrocytes subsequently flattened out and formed orderly columns of flat chondrocytes in which *11Prom-Cre* directs recombination (Iwai et al., 2008).

Histological analysis showed that *11Prom-Cre; Sox9$^{flox/flox}$* conditional knockout mice form primordial cartilage normally in the humerus and a normal Sox9 expression pattern is present at 13.0 dpc (Fig. 2C). At 13.5 dpc, the humerus of *Sox9$^{flox/+}$* control mice showed prehypertrophy and hypertrophy of chondrocytes in the central region of cartilage primordia. Proliferative chondrocyte-specific expression of Sox9 abruptly stopped when chondrocytes entered into the prehypertrophic stage in control mice. The length (proximodistal direction) of the zone of proliferative chondrocytes expressing Sox9 in *11Prom-Cre; Sox9$^{flox/flox}$* humerus was 25% shorter than that in *Sox9$^{flox/+}$* control humerus (Fig. 2D, arrows). These results suggest that Sox9 expression was lost in several layers of flat chondrocytes closest to the prehypertrophic chondrocytes in *11Prom-Cre; Sox9$^{flox/flox}$* humerus.

The width (transverse direction) of the central region of the primordial cartilage was decreased in *11Prom-Cre; Sox9$^{flox/flox}$* mouse humerus at 13.5 dpc, and the humerus had a dumb-bell-shaped appearance (Fig. 2D,E). The dumb-bell shape was confirmed by Alcian Blue staining of the skeleton at 14.5 dpc (Fig. 2F). The zone of hypertrophic chondrocytes and the zone of terminally mature chondrocytes were formed in the center of *Sox9$^{flox/+}$* control humerus at 14.5 dpc. By contrast, the hypertrophic chondrocytes were absent and cells that resembled terminally mature chondrocytes were present in the center of the *11Prom-Cre; Sox9$^{flox/flox}$* humerus (Fig. 2G).

11Prom-Cre; Sox9$^{flox/flox}$ flat chondrocytes undergo prehypertrophy, skip hypertrophy and undergo vigorous apoptosis

We analyzed the expression of marker genes at 13.5 dpc. The expression pattern of *Col2a1* mRNAs (Fig. 3A) corresponded almost exactly to that of Sox9 proteins in *11Prom-Cre; Sox9$^{flox/flox}$* humerus (Fig. 2D). *Ppr* (receptor for parathyroid hormone and parathyroid hormone-related peptides; *Pth1r* – Mouse Genome Informatics) mRNAs were detected in *11Prom-Cre; Sox9$^{flox/flox}$* humerus (Fig. 3A). Hypertrophic chondrocyte marker type X collagen (*Col10a1*) mRNA was detected in the center of *Sox9$^{flox/+}$* cartilage, but not in *11Prom-Cre; Sox9$^{flox/flox}$* cartilage. *Runx2* mRNA was strongly detected in bone collars of primordial cartilage and weakly detected in chondrocytes in *Sox9$^{flox/+}$* humerus. *Runx2* expression in chondrocytes appeared to increase in *11Prom-Cre; Sox9$^{flox/flox}$* humerus. The bone collar was thickened and type I collagen expression in the bone collar increased in *11Prom-Cre; Sox9$^{flox/flox}$* humerus. The distances (Fig. 3B, black arrows) between the distal articular surface and prehypertrophic zone indicated by *Ihh* expression were reduced in *11Prom-Cre; Sox9$^{flox/flox}$* humerus (Fig. 3B, bar chart). The distance (Fig. 3B, white arrows) between the two zones of *Ihh*-positive cells was increased in *11Prom-Cre; Sox9$^{flox/flox}$* humerus. These results, together with the Sox9 expression patterns (Fig. 2D), suggest that the premature shutdown of Sox9 in several cell layers of flat chondrocytes caused a shift of *Ihh* expression toward the articular surfaces of primordial cartilage and an absence of *Col10a1* expression.

The abnormalities found in *11Prom-Cre; Sox9$^{flox/flox}$* cartilage at 13.5 dpc were enhanced at 14.5 dpc. In control *Sox9$^{flox/+}$* humerus, flat chondrocytes, which had emerged next to prehypertrophic chondrocytes at 13.5 dpc, dramatically increased in number in the metaphyseal zones at 14.5 dpc. The number of chondrocytes in the metaphyseal zone of *11Prom-Cre; Sox9$^{flox/flox}$* humerus was decreased as compared with the control *Sox9$^{flox/+}$* humerus (see Fig. S4A in the supplementary material, top row, outlined region). Sox9 expression was only detected in epiphyseal round chondrocytes in *11Prom-Cre; Sox9$^{flox/flox}$* humerus, whereas Sox9 was expressed both in epiphyseal round and metaphyseal flat chondrocytes in the control *Sox9$^{flox/+}$* humerus. These results indicate that metaphyseal proliferative chondrocytes in *11Prom-Cre; Sox9$^{flox/flox}$* humerus are *Sox9$^{floxdel/floxdel}$* proliferative chondrocytes (see Fig. S4A in the supplementary material, right panels, outlined region). The expression patterns of *Col2a1* and *Col11a2* corresponded to those of Sox9 proteins. *Ppr* was expressed, but *Col10a1* expression was lost in *11Prom-Cre; Sox9$^{flox/flox}$* cartilage. Real-time RT-PCR analysis of RNA from the humerus confirmed a significant decrease in *Col10a1* expression (Fig. 3C).

Col1a1 mRNAs and proteins were ectopically expressed in the chondrocytes in the central region of *11Prom-Cre; Sox9$^{flox/flox}$* humeral cartilage at 14.5 dpc (Fig. 3D). Together with the cell morphology (Fig. 2G, TC-L), the expression of *Mmp13*, bone sialoprotein (*Bsp*; *Ibsp* – Mouse Genome Informatics) mRNA and osteopontin (*Op*; *Spp1* – Mouse Genome Informatics) mRNA (Fig. 3D) strongly suggest that these cells are terminally mature chondrocytes. The absence of *Col10a1*-expressing cells and the reduced number of *Mmp13*-, *Bsp*- and *Op*-expressing cells suggest that *Sox9* deletion in flat chondrocytes severely inhibits subsequent hypertrophy and moderately inhibits terminal maturation. Mineralization of chondrocytes in the central region of the cartilage was increased. Cells were TUNEL negative and did not show immunoreactivity for cleaved caspase 3 in *11Prom-Cre; Sox9$^{flox/flox}$* humerus at 13.5 dpc (see Fig. S4B in the supplementary material). Significant apoptosis associated with the expression of cleaved caspase 3 was detected in the zone of terminally mature chondrocytes (Fig. 3E) at 14.5 dpc. These results suggest that *Sox9* deletion started in flat chondrocytes at 13.5 dpc and that chondrocytes lacking Sox9 undergo abnormal differentiation (severe inhibition of hypertrophy and moderate inhibition of terminal differentiation) into terminally mature chondrocytes, where excess apoptosis is detected at 14.5 dpc.

BrdU labeling analysis (see Fig. S4C in the supplementary material) revealed increased proliferation of perichondrial bone collar cells in *11Prom-Cre; Sox9$^{flox/flox}$* humeral cartilage at 13.5 dpc; this increased proliferation was responsible for the thick bone collar (Fig. 2D). Proliferation rates in metaphyseal zone chondrocytes in *11Prom-Cre; Sox9$^{flox/flox}$* humeral cartilage decreased at 14.5 dpc; this decreased proliferation caused a corresponding decrease in the length of the zone of metaphyseal chondrocytes (see Fig. S4A in the supplementary material).

Our results indicate that flat chondrocytes lacking Sox9 expression are characterized by the cessation of *Col2a1* expression, decreased proliferation rates, a reduced cell population, a shift of prehypertrophy towards the articular end, and a lack of hypertrophy; these chondrocytes immediately enter into terminal maturation associated with ectopic type I collagen expression in the cartilage matrix, undergo increased apoptosis and stimulate the proliferation of bone collar cells. Thus, Sox9 is needed for subsequent chondrocyte hypertrophy. This phenotype is similar to those of *Sox5$^{-/-}$; Sox6$^{-/-}$* (Smits et al., 2001), *Sox5$^{+/-}$;Sox6$^{-/-}$* and *Sox5$^{-/-}$;Sox6$^{+/-}$* mice (Smits et al., 2004). *Sox5$^{-/-}$; Sox6$^{-/-}$* mice lack columnar chondrocytes and *Col10a1* expression, but they do have prehypertrophic

chondrocytes and express *Mmp13*. Because Sox5 and Sox6 facilitate the organization of transcription complexes (Lefebvre and Smits, 2005), the phenotypic similarities between *11Prom-Cre; Sox9*$^{flox/flox}$ mice and *Sox5*$^{-/-}$; *Sox6*$^{-/-}$ mice suggest that the *Sox9* conditional knockout phenotype is due to dysfunction of transcription complexes containing Sox5, Sox6 and Sox9. The observation that chondrocytes lacking Sox9 enter into terminal maturation without hypertrophy is consistent with findings that Sox9 misexpression in hypertrophic chondrocytes inhibits their terminal maturation (Hattori et al., 2010).

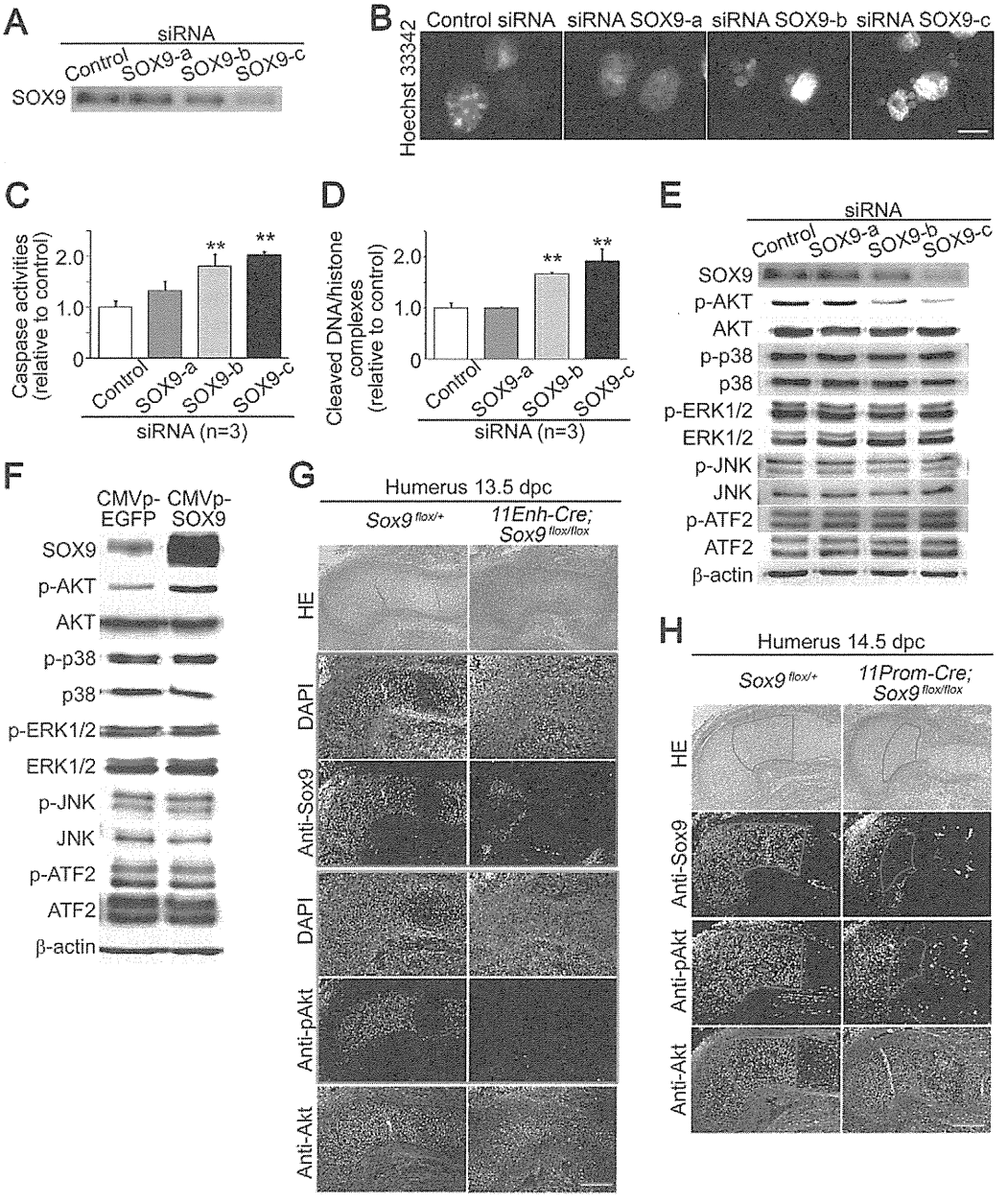

Fig. 4. Apoptosis of SW1353 chondrosarcoma cells by SOX9 knockdown and Akt phosphorylation in SW1353 cells and mice. (**A**) Immunoblot analysis of SOX9 expression in human SW1353 chondrosarcoma cells transfected with either of three different sets of SOX9 siRNAs (Invitrogen). Control shows Stealth RNAi negative control (Invitrogen). (**B**) Hoechst-stained SW1353 cells transfected with each siRNA. (**C**) Transfection with siRNA SOX9-b or siRNA SOX9-c increased caspase 3/7 activities in SW1353 cells. (**D**) Transfection with siRNA SOX9-b or siRNA SOX9-c increased the amount of cleaved DNA-histone complexes in SW1353 cells. Data (C,D) are mean + s.d. **, $P<0.01$. (**E**) Immunoblot analysis of SW1353 cells transfected with SOX9 siRNAs. (**F**) Immunoblot analysis of SW1353 cells transfected with either CMV promoter-EGFP (control) or CMV promoter-SOX9 (SOX9 overexpression). (**G**) Semi-serial sections of *Sox9*$^{flox/+}$ and *11Enh-Cre; Sox9*$^{flox/flox}$ samples as shown in Fig. 1C stained with HE or DAPI or immunostained for Sox9, Akt or phosphorylated (p) Akt. Sections immunostained with anti-Sox9 and anti-pAkt were double stained with DAPI, showing that these two sections are comparable. (**H**) Semi-serial sections of *Sox9*$^{flox/+}$ and *11Prom-Cre; Sox9*$^{flox/flox}$ humerus at 14.5 dpc. Metaphyseal flat proliferative chondrocytes are outlined (red line) in *Sox9*$^{flox/+}$ humerus (left panels). Metaphyseal proliferative chondrocytes that did not express Sox9, indicating that their *Sox9* gene was deleted (*Sox9*$^{flodelx/floxdel}$ chondrocytes), are outlined in *11Prom-Cre; Sox9*$^{flox/flox}$ humerus (right panels). *Sox9*$^{flodelx/floxdel}$ proliferative chondrocytes showed decreased immunoreactivity to anti-pAkt as compared with flat proliferative chondrocytes in control *Sox9*$^{flox/+}$ mice. Scale bars: 10 μm in B; 200 μm in G,H.

SOX9 knockdown-induced apoptosis of SW1353 chondrosarcoma cells

Next, we examined whether Sox9 is important for the survival of chondrosarcoma cells in vitro. To knockdown *SOX9* mRNA, we transfected human SW1353 chondrosarcoma cells with small interfering RNA (siRNA) using the Amaxa nucleofection technique, which yields high transfection efficiencies (see Fig. S5A in the supplementary material), and harvested the cells 6 hours later. SW1353 cells transfected with SOX9-c siRNA showed a dramatic decrease in SOX9 protein, whereas SOX9-b siRNA yielded a moderate decrease and SOX9-a siRNA did not affect the level of SOX9 protein (Fig. 4A). Hoechst-stained SW1353 cells transfected with siRNA SOX9-b and siRNA SOX9-c exhibited typical apoptotic morphology characterized by chromatin condensation and DNA fragmentation (Fig. 4B). The decrease in SOX9 expression (Fig. 4A) correlated with the increase in caspase 3/7 activities (Fig. 4C) and the amount of cleaved DNA-histone complexes (nucleosomes) (Fig. 4D) in SW1353 cells. These results suggest that the cell survival mechanism that requires SOX9 is also active in SW1353 chondrosarcoma cells. A possible explanation for the rapid death of SW1353 cells is that these chondrosarcoma cells undergo rapid cell cycles, such that the outcome of loss of SOX9 is quickly realized. Transfection of human HeLa cells or osteoblastic Saos2 cells with SOX9 siRNAs did not cause apoptosis; this result is consistent with the lack of SOX9 expression in these cell types (see Fig. S5B-D in the supplementary material). Thus, Sox9 is specifically needed for the survival of chondrocyte lineage cells, including chondrocytes and chondrosarcoma cells.

Akt phosphorylation is involved in the chondrocyte apoptosis induced by *Sox9* deletion

We next investigated the molecular mechanism of Sox9-induced survival of chondrocyte lineage cells. We first examined the activation of signaling molecules in SW1353 chondrosarcoma cells by western blot analysis. SOX9 knockdown specifically decreased the phosphorylation level of AKT, but it did not affect the phosphorylation levels of p38 mitogen-activated protein kinase (p38 MAPK; MAPK14 – Human Genome Nomenclature Committee), extracellular signal-regulated kinase (ERK), Jun N-terminal kinase (JNK) and activating transcription factor 2 (ATF2) (Fig. 4E). Consistently, the overexpression of SOX9 specifically increased the phosphorylation level of AKT, but did not change the phosphorylation levels of other signaling molecules (Fig. 4F).

We then examined phosphorylation in vivo. Immunohistochemical analysis showed that phospho-Akt was below detectable levels in both the control $Sox9^{flox/+}$ and *11Enh-Cre;* $Sox9^{flox/flox}$ mice at 12.5 dpc (Fig. S5E in the supplementary material). Phospho-Akt was detected in the central part of primordial cartilage and not in the periphery, whereas Sox9 was detected both in the central and peripheral parts of primordial cartilage in the control $Sox9^{flox/+}$ mice at 13.5 dpc (Fig. 4G). The area of *Sox9* deletion was limited to the central part of cartilage in *11Enh-Cre;* $Sox9^{flox/flox}$ mice and appeared to cover the area of phospho-Akt in the control $Sox9^{flox/+}$ mice at 13.5 dpc. Phospho-Akt was not detected in *11Enh-Cre;* $Sox9^{flox/flox}$ cartilage at 13.5 dpc (Fig. 4G), nor in $Sox9^{floxdel/floxdel}$ proliferative chondrocytes in *11Prom-Cre;* $Sox9^{flox/flox}$ mice (Fig. 4H). There were no obvious differences in the levels of phosphorylated Atf2, Jnk or p38 Mapk, as detected by antibody, between $Sox9^{floxdel/floxdel}$ proliferative chondrocytes in *11Prom-Cre;* $Sox9^{flox/flox}$ mice and proliferating chondrocytes in $Sox9^{flox/+}$ mice (see Fig. S5F in the supplementary material).

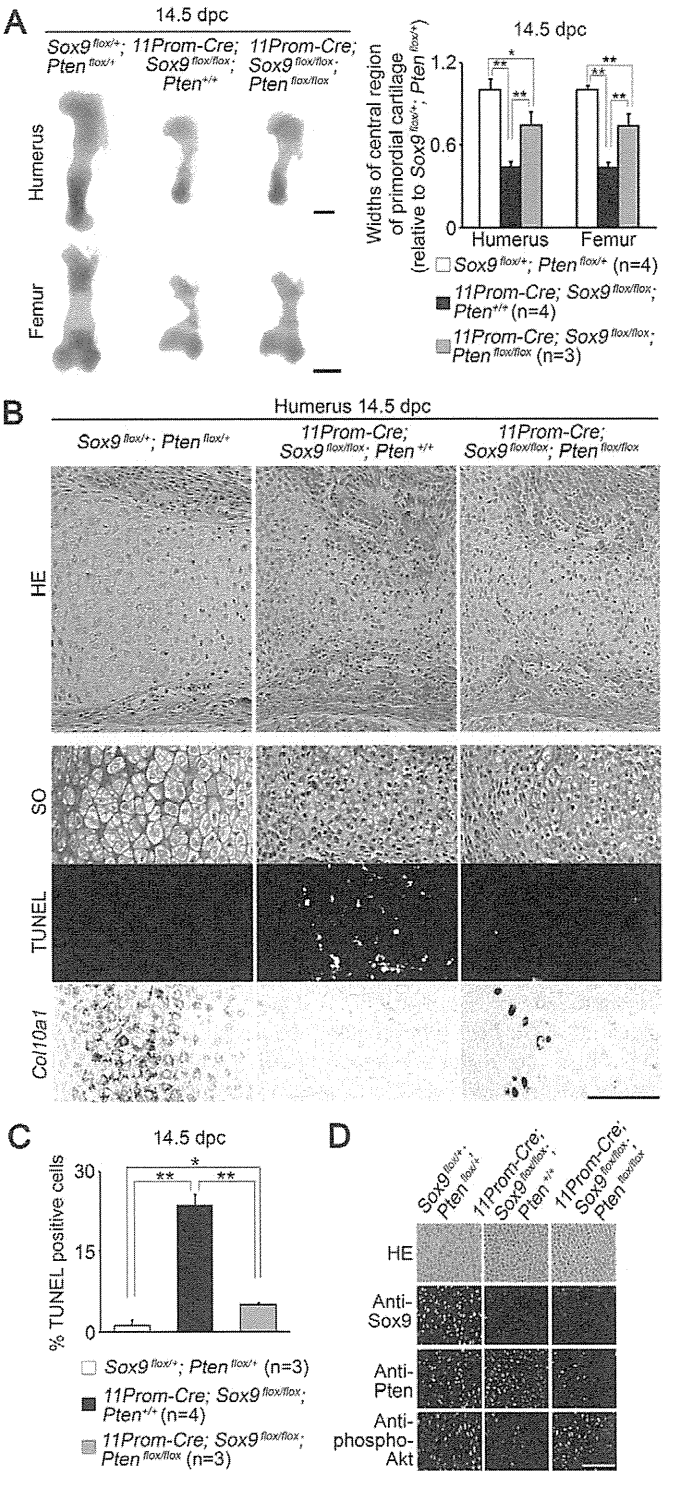

Fig. 5. Inactivation of *Pten* partially rescues the survival of $Sox9^{floxdel/floxdel}$ chondrocytes and *Col10a1* expression. (**A**) Humeral and femoral cartilaginous mouse skeletons at 14.5 dpc stained with Alcian Blue. (**B**) Central regions of the humerus at 14.5 dpc stained with HE or SO, hybridized with *Col10a1* cRNA probe or subjected to the TUNEL assay, as labeled. (**C**) The percentage of TUNEL-positive cells among the total cell number. (**D**) Sox9, Pten and pAkt immunohistochemistry of proliferative chondrocytes in the metaphyseal regions of the humerus from mice of the indicated genotypes. Data (A,C) are mean + s.d. *, $P<0.05$; **, $P<0.01$. Scale bars: 200 μm in A; 100 μm in B,D.

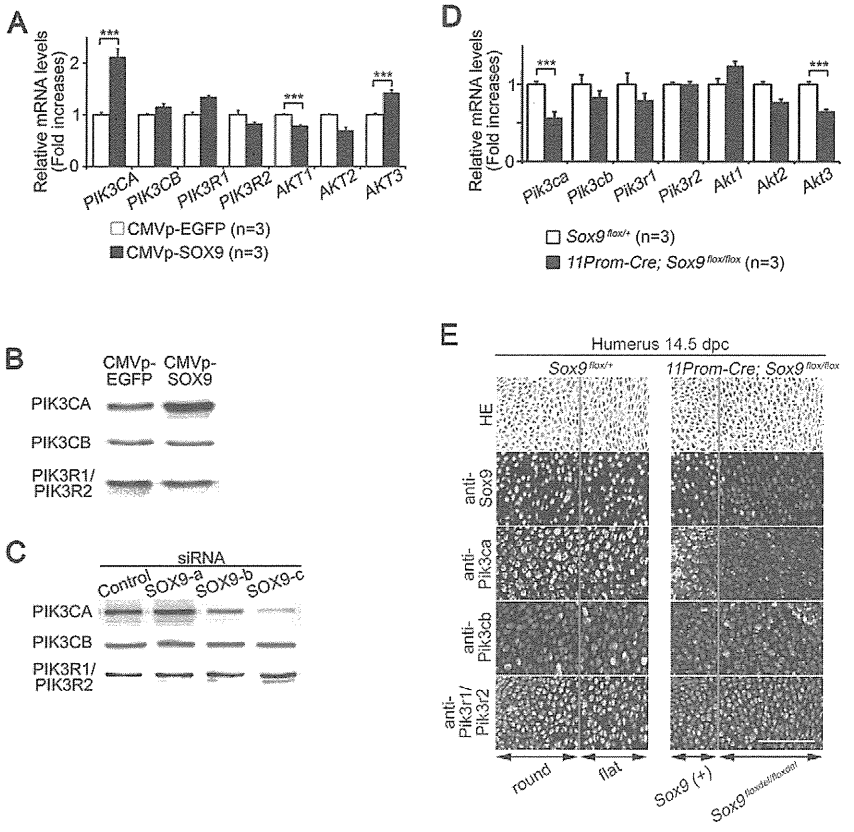

Fig. 6. Regulation of expression of *PIK3CA* by Sox9. (**A**) Real-time RT-PCR analysis of PIK3 and AKT gene expression in human SW1353 cells transfected with CMV promoter-EGFP (control) or CMV promoter-SOX9 (SOX9 overexpression). The expression levels of the genes in cells transfected with CMV promoter-EGFP were set at 1. (**B**) Immunoblot analysis of SW1353 cells transfected with CMV promoter-EGFP (control) or CMV promoter-SOX9 (SOX9 overexpression). (**C**) Immunoblot analysis of SW1353 cells transfected with SOX9 siRNA. Degrees of SOX9 knockdown by each siRNA are shown in Fig. 4A. (**D**) Real-time RT-PCR analysis of humerus from *Sox9*$^{flox/+}$ and *11Prom-Cre; Sox9*$^{flox/flox}$ mice. The expression levels of the genes in *Sox9*$^{flox/+}$ humerus were set at 1. Data (A,D) are mean + s.d. ***, $P<0.0001$. (**E**) HE staining and immunohistochemistry for the indicated proteins (green) counterstained with DAPI (blue) in proximal humeral cartilage at 14.5 dpc. (Left) For cartilage of *Sox9*$^{flox/+}$ mice, the red line indicates the transition between the round and flat proliferative chondrocyte zones. Sox9, Pik3ca, Pik3cb and Pik3r1/Pik3r2 were expressed both in round and flat proliferative chondrocytes. (Right) In cartilage of *11Prom-Cre; Sox9*$^{flox/flox}$ mice, anti-Sox9 revealed a boundary (red line) between chondrocytes in which the *Sox9* gene was not deleted and was expressed [*Sox9* (+)] and chondrocytes in which the *Sox9* gene was deleted and was not expressed (*Sox9*$^{floxdel/floxdel}$). Immunoreactivity against anti-Pik3ca decreased in *Sox9*$^{floxdel/floxdel}$ chondrocytes. Scale bar: 50 μm.

We next examined whether reduced phosphorylation of Akt is responsible for *Sox9* deletion-mediated chondrocyte apoptosis. We prepared *11Prom-Cre; Sox9*$^{flox/flox}$; *Pten*$^{flox/flox}$ double conditional knockout mice. Pten (phosphatase and tensin homolog) is a lipid phosphatase, the major substrate of which is PtdIns(3,4,5)P_3. Thus, the deletion of *Pten* results in the accumulation of PtdIns(3,4,5)P_3, leading to forced activation of Akt. *Col2a1-Cre; Pten*$^{flox/flox}$ mice show increased phosphorylation of Akt (Ford-Hutchinson et al., 2007; Yang et al., 2008). At 14.5 dpc, Alcian Blue staining of the skeleton showed that the degree of deformity of humeral cartilage in *11Prom-Cre; Sox9*$^{flox/flox}$; *Pten*$^{flox/flox}$ mice was milder than that in *11Prom-Cre; Sox9*$^{flox/flox}$; *Pten*$^{+/+}$ mice (Fig. 5A). The constriction of central regions of the humerus was also significantly milder. Histological analysis showed that the decreased cell numbers in the center of the cartilage, the excess number of TUNEL-positive cells and the loss of *Col10a1* expression in *11Prom-Cre; Sox9*$^{flox/flox}$; *Pten*$^{+/+}$ mice were partly restored in *11Prom-Cre; Sox9*$^{flox/flox}$; *Pten*$^{flox/flox}$ mice (Fig. 5B,C). Pten expression was decreased in *Sox9*$^{floxdel/floxdel}$; *Pten*$^{floxdel/floxdel}$ proliferative chondrocytes in *11Prom-Cre; Sox9*$^{flox/flox}$; *Pten*$^{flox/flox}$ mice (Fig. 5D and see Fig. S6 in the supplementary material). Phosphorylation levels of Akt in *Sox9*$^{floxdel/floxdel}$; *Pten*$^{floxdel/floxdel}$ proliferative chondrocytes were higher than those of *Sox9*$^{floxdel/floxdel}$; *Pten*$^{+/+}$ proliferative chondrocytes. Thus, both *Sox9* deletion and elevated Akt phosphorylation occurred in flat chondrocyte regions and the resulting modulation of apoptosis became apparent subsequently, when cells differentiated into terminally mature chondrocytes. These results suggest that decreased *Col10a1* expression and increased apoptosis induced by *Sox9* deletion are partly restored by the additional deletion of *Pten*, which restores Akt phosphorylation.

Regulation of expression of Pik3ca by Sox9

We used expression analysis and the candidate approach to investigate the molecular mechanism underlying the regulation of Akt phosphorylation by Sox9. We found that the expression of Pik3ca was regulated by Sox9. Pik3ca (also known as p110α) is one of three subunit proteins of phosphatidylinositol 3-kinase (PI3K). PI3K generates phosphatidylinositol (3,4,5)-trisphosphate [PtdIns(3,4,5)P_3] from PtdIns(4,5)P_2. PtdIns(3,4,5)P_3 causes phosphorylation of and activates Akt (Brazil et al., 2004). PI3K-Akt signaling regulates cell death (Cantley, 2002).

The regulation of PIK3CA expression by SOX9 was detected in SW1353 chondrosarcoma cells in vitro. Among genes encoding PI3K subunits, *PIK3CA* mRNA was induced by SOX9 overexpression (Fig. 6A). The expression levels of genes encoding the other PI3K subunits and AKT members were little affected by SOX9 overexpression. *PIK3CG* and *PIK3CD* (also known as *p110*γ and *p110*δ, respectively) mRNAs were not detected in SW1353 cells. Western blot analysis of SW1353 cell lysates showed that SOX9 overexpression increased PIK3CA protein levels but did not affect PIK3CB (p110β) or PIK3R1 (p85α)/PIK3R2 (p85β) protein levels (Fig. 6B). Consistently, SOX9 knockdown decreased PIK3CA protein levels but did not affect PIK3CB or PIK3R1/PIK3R2 protein levels (Fig. 6C).

The Sox9-mediated regulation of *Pik3ca* expression was also detected in vivo. Real-time RT-PCR analysis confirmed that *Pik3ca* expression was significantly decreased in *11Prom-Cre; Sox9*$^{flox/flox}$ humeral cartilage as compared with the expression level in control *Sox9*$^{flox/+}$ cartilage (Fig. 6D). Immunohistochemical analysis showed that Pik3ca immunoreactivity decreased in proliferative chondrocytes that did not express Sox9 (*Sox9*$^{floxdel/floxdel}$) as